https://doi.org/10.5194/egusphere-2026-556
Preprint. Discussion started: 17 March 2026

A framework for evaluating ice sheet altimetry uncertainty estimates

Karla Boxall[1], Malcolm McMillan[1], Alan Muir[2], Sarah Appleby[3], Sophie Dubber[3], Noel Gourmelen[4], Clare Willis[1], Joe Phillips[1]

[1] UK Centre for Polar Observation and Modelling, Centre of Excellence in Environmental Data Science, Lancaster University, Lancaster, UK
[2] Mullard Space Science Laboratory, University College London, London, UK
[3] Earthwave Ltd., Edinburgh, UK
[4] University of Edinburgh, Edinburgh, UK

Correspondence to: Karla Boxall (k.boxall@lancaster.ac.uk)

Abstract. For three decades, ice sheet elevation records from satellite radar altimetry have provided new insight into the state of the cryosphere and its contribution to global sea-level rise. The availability of robust, consistent and traceable uncertainties alongside ice sheet elevation data is crucial for combining measurements across missions and enabling their use in reconciling estimates of ice sheet mass balance and constraining numerical ice sheet models. At present, such uncertainties are largely absent from existing Level 2 ice sheet elevation products, and for the subset of products where uncertainties are provided, there is neither a standardised approach to uncertainty generation nor a method to evaluate their robustness. Here, we develop a novel uncertainty evaluation framework and provide a comprehensive assessment of uncertainty generation for altimetry-based ice sheet elevations. Overall, we find that calculating uncertainty as a parameterisation of topographic complexity (characterised by surface slope and roughness) and measurement quality (characterised by backscattered power and coherence) improves performance relative to solutions that use fewer co-variates. Ultimately, the framework presented here will enable the systematic characterisation of ice sheet elevation uncertainties associated with historical, current and future polar radar altimeter missions, including the Copernicus Polar Ice and Snow Topography Altimeter (CRISTAL). Such information will aid the successful combination of altimetry measurements across missions, improve the constraint of numerical ice sheet models, and enable more certain estimates of current and future ice sheet mass balance and global sea-level rise.

1. Introduction

Satellite radar altimeters have provided a largely uninterrupted record of ice sheet elevation in the polar regions for more than a quarter of a century. By resolving comprehensive signals of elevation change at a kilometre-scale spatial resolution, satellite radar altimetry has enabled the large-scale monitoring of the Antarctic and Greenland ice sheets (Konrad et al., 2017; Shepherd et al., 2019; Suryawanshi et al., 2025). Specifically, the launch of satellite altimeters carrying conventional pulse-limited radar instruments (ERS-1, ERS-2, Envisat, AltiKa), those capable of Synthetic Aperture Radar (SAR) processing (Sentinel-3), and those with SAR interferometric capability (CryoSat-2), have provided detailed topographical information (Remy et al., 1989; Bamber and Bindschadler, 1997; Bamber et al., 2009; Helm et al., 2014), alongside accurate

https://doi.org/10.5194/egusphere-2026-556
Preprint. Discussion started: 17 March 2026

estimations of ice sheet volume (Davis and Ferguson, 2004; Johannessen et al., 2005) and mass change (Wingham et al., 2006a; Zwally et al., 2011; Shepherd et al., 2012; McMillan et al., 2014; 2016). The latter, together with estimates of ice thickness, surface mass balance and flow (Moon et al., 2012; Mouginot et al., 2017; Gardner et al., 2018) and changes in Earth's gravity field (Tapley et al., 2019; Velicogna et al., 2020; Sasgen et al., 2020), have contributed to reconciled estimates of ice sheet mass balance (The IMBIE Team, 2018; 2020; Otosaka et al., 2022). Altimetry-derived ice sheet elevation estimates (McMillan et al., 2014; Sørensen et al., 2015; Schröder et al., 2019; Nilsson et al., 2022) have also improved process-based understanding of subglacial hydrology (Smith et al., 2017; Siegfried and Fricker, 2018; Malczyk et al., 2020) and the ice-ocean interface (Adusumilli et al., 2020; Davison et al., 2022; Gourmelen et al., 2025).

To capitalise fully on the extensive value of satellite altimetry, it is necessary for robust and traceable uncertainties to be provided alongside ice sheet elevation measurements, where uncertainty represents the potential deviation between the retrieved elevation and the true surface height. In the context of numerical ice sheet modelling, for example, interpretable uncertainties are a key constraint when estimating current and future ice sheet behaviour (Hebeler et al., 2008). In parallel, consistent and well-characterised uncertainties are required across coincident altimetry missions for the development of formal data assimilation frameworks. At present, uncertainties are absent from the standard CryoSat-2 ground segment (ESA, 2023a; 2023b) and from existing Sentinel-3 ice sheet elevation products (ESA, 2025a). Transparent, traceable uncertainties are provided within the CryoSat-2 TheMatic PrOduct (Cryo-TEMPO) Point of Closest Approach (POCA) product (ESA, 2025b) and the Cryo-TEMPO Elevation Over Land Ice from Swath (EOLIS) product (ESA, 2019) but are produced using differing methodologies. The scarcity of existing uncertainties, compounded by their lack of standardisation, necessitates the development of a novel framework for evaluating the uncertainties of altimetry-based ice sheet elevations. Such a framework would enable, for the first time, an assessment of the extent to which new and existing uncertainties characterise the true accuracy of the ice sheet elevation measurements.

In this study, we develop a new framework for evaluating the performance of uncertainties generated for radar altimetry-based ice sheet elevation measurements. We apply this framework to intercompare existing methods of uncertainty generation associated with the CryoSat-2 Cryo-TEMPO POCA and Cryo-TEMPO EOLIS products. Next, we show how the framework can be used as the basis for developing new uncertainties for datasets currently lacking such information; in this case the Sentinel-3 thematic land ice product.

2. Uncertainty Evaluation Framework

Currently, there exists no approach within the ice sheet community for assessing the robustness of altimetry-derived ice elevation uncertainties. This study develops a framework to assess numerous methods of uncertainty generation for the

https://doi.org/10.5194/egusphere-2026-556
Preprint. Discussion started: 17 March 2026

purpose of evolving, optimising and harmonising existing approaches, and for evaluating their application to existing and upcoming altimeter-derived products.

Here, we present our framework for uncertainty assessment that evaluates the extent to which the calculated uncertainty values adequately capture the true deviation from an unseen reference dataset. To this end, we generate an uncertainty lookup table using data spanning a full year (nominally 2020) (further details on the approach are provided in Section 3.2.1). The uncertainty lookup table is then used to assign uncertainties to elevation measurements spanning 2022, which are compared to a set of unseen, co-located elevation differences that are generated with respect to a reference dataset. The similarity between the uncertainty values and the unseen elevation differences are assessed in two stages.

In the first stage of the framework, the overall distribution of all elevation differences from our unseen (2022) dataset is compared to the corresponding distribution of uncertainty values. Closely matching distributions indicate that the overall distribution of uncertainties is realistic at an aggregated ice sheet scale, which is a desirable characteristic, but do not provide more granular details relating to the appropriateness of the uncertainties associated with individual points. Distribution similarity is quantified through comparison of their median and upper/lower quartiles as the distributions are typically non-Gaussian.

In the second stage of the framework, for each co-located elevation difference measurement, the residual to the uncertainty is calculated, as shown below:

$$resid = \left|E_{alt,i} - E_{ref,i}\right| - \sigma_i \qquad (1)$$

where $E_{alt,i}$ and $E_{ref,i}$ are the ith pair of altimeter and reference elevations, respectively, and σ_i is the uncertainty associated with the ith elevation measurement, as derived from our lookup table. The distribution of residuals reflects the proportion of measurements where the uncertainty value under- or over-estimates the actual magnitude of the difference relative to a reference measurement, whereby negative (positive) residuals represent over- (under-)estimated uncertainty values. An assessment of the distribution of residuals is made according to their centrality and width. It is preferable for the distribution to have a narrow peak centred close to zero, indicating a close correspondence between individual uncertainty and elevation difference values. The median residual value denotes the deviation from a zero-centred distribution (i.e. overall tendency to over- or under-estimate uncertainty), while the interquartile range (IQR) is representative of the width of the peak (i.e. overall characterisation of the magnitude of over- or under-estimation).

https://doi.org/10.5194/egusphere-2026-556
Preprint. Discussion started: 17 March 2026

3. Data and methods

3.1 Data

3.1.1 Altimetry data

As introduced in Section 1, the uncertainty evaluation framework is applied, first, to intercompare existing methods of uncertainty generation, focussing on data acquired by CryoSat-2. Second, the framework is used as the basis for developing new uncertainties for Sentinel-3 datasets currently lacking assigned uncertainties.

Towards the first aim, the framework is utilised to compare and align the approaches to uncertainty generation taken by Cryo-TEMPO POCA and Cryo-TEMPO EOLIS (Section 3.2.1). To this end, we use ESA CryoSat-2 L2 in-depth (L2I) Baseline E data (Figure B1a; ESA, 2023b) in place of the Cryo-TEMPO POCA dataset to generate the uncertainties owing to the necessity to include additional co-variate parameters, such as backscattered power and interferometric coherence, which are inherent to the L2I dataset. For the swath processed data, we use the Cryo-TEMPO EOLIS data (Figure B1b; Gourmelen et al., 2018; ESA, 2019). Uncertainty lookup tables are generated separately for Antarctica and Greenland using elevation data spanning 2020, and later used to assign uncertainties to elevation measurements in 2022 (Section 2). Analysis was conducted over regions where CryoSat-2 operates in SAR Interferometric (SARIn) mode only as Cryo-TEMPO EOLIS data is unavailable elsewhere and both datasets were required for inter-comparison purposes.

Towards the second aim, we use ESA Sentinel-3 Level-2 Hydro-Cryo Thematic products BC-005 data (Figure B1c; ESA, 2025a) to generate and evaluate ice sheet elevation uncertainties for the first time. As above, uncertainty lookup tables are generated separately for Antarctica and Greenland using all available elevation data acquired over the ice sheets in 2020. Uncertainties were later assigned to Sentinel-3 Level-2 thematic ice sheet elevation measurements in 2022 (Section 2).

3.1.2 Reference data

The reference data consist of ICESat-2 ATL-06 v006 land-ice surface height measurements (Smith et al., 2023). When generating the uncertainties, the ICESat-2 data are co-located in space and time to the altimetry measurements acquired in 2020 (Section 3.2.1). To evaluate the uncertainties, co-located ICESat-2 data acquired in 2022 are used as the unseen reference dataset (Section 2).

ICESat-2 was chosen as the reference dataset owing to its comprehensive ice-sheet-wide coverage with a 91-day repeat cycle at a high along-track spatial resolution of ~20 m, and its temporally overlapping availability with CryoSat-2 data. The geolocated ice surface heights are assumed to represent the truth owing to the centimetre-scale precision and several-metre horizontal positioning accuracy provided by the six lidar beams arranged as three pairs. Specifically, comparisons with GNSS data have shown the accuracy of ALT06 to be <3.3 cm, with a surface measurement precision of <7.2 cm over the ice

https://doi.org/10.5194/egusphere-2026-556
Preprint. Discussion started: 17 March 2026

sheet interior (Brunt et al., 2019; 2021), with an accuracy of 1.5 cm and a precision of 9.1 cm over a test zone covering a variety of Antarctic ice surface conditions (Li et al., 2021).

3.1.3 Auxiliary data

Several auxiliary datasets are required for the generation of uncertainties, specifically when binning elevation differences in the construction of the lookup table (Section 3.2.1). In this study, the use of up to four co-variates is assessed. Similar to the approach taken by Cryo-TEMPO EOLIS (Section 3.2.1), the co-variates tested include combinations of surface slope, surface roughness and power; plus coherence for CryoSat-2 interferometric acquisitions, as these variables have been shown to impact the quality of radar altimetry-derived elevations.

The slope and roughness data used to generate all uncertainties assessed in this study were derived for the Antarctic Ice Sheet using the REMA v2.0 100 m resolution DEM mosaic (Howat et al., 2022) and for the Greenland Ice Sheet using the ArcticDEM v4.1 100 m resolution DEM mosaic (Porter et al., 2023). At each elevation point, a best-fit plane was estimated using Singular Value Decomposition (SVD) applied to a 9x9-pixel neighbourhood (900x900 m). Slope was computed as the magnitude of the plane's gradient (in degrees) (Figure B2a, c), and roughness as the standard deviation of the orthogonal residuals from the fitted plane (in metres) (Figure B2b, d) (Phillips and McMillan, 2024). This approach explicitly decouples slope from roughness, avoiding the artificial correlation introduced by conventional methods that measure local elevation variance without accounting for topographic inclination (Phillips and McMillan, 2024). The remaining auxiliary data, namely coherence (Figure B1d) and backscattered power (Figure B1e-f), are provided in the Level-2 data (Section 3.1.1).

3.2 Methods

3.2.1 Existing approaches to uncertainty estimation

Within the context of existing ice sheet altimetry processing chains, two CryoSat-2-derived Level-2 products include uncertainty estimates alongside ice elevation measurements: the Cryo-TEMPO Point of Closest Approach (POCA) product (ESA, 2025b), and the Cryo-TEMPO Elevation Over Land Ice from Swath (EOLIS) product (ESA, 2019). Here, we briefly review the approaches taken towards uncertainty estimation by each of these processing chains to identify potential opportunities for refining the existing methodologies.

The approach taken by both Cryo-TEMPO POCA and Cryo-TEMPO EOLIS to estimate the uncertainty of ice sheet elevation retrievals is based upon an empirical parameterisation of the difference in elevation relative to a reference measurement, where the parameterisation is based upon a set of auxiliary variables. An empirical, "top-down" approach to uncertainty estimation is taken, rather than a formal, "bottom-up" propagation of uncertainties from Level 0 or 1 data, as the latter does not currently exist.

https://doi.org/10.5194/egusphere-2026-556
Preprint. Discussion started: 17 March 2026

For the Cryo-TEMPO POCA product, the elevation difference to a reference dataset is parameterised as a function of surface slope and, optionally, roughness, while for Cryo-TEMPO EOLIS, the elevation difference is parameterised as a function of across-track slope, along-track slope, roughness, power, coherence and distance to POCA. These approaches are based upon the understanding that radar altimeter measurement accuracy is sensitive to each of these variables, with surface slope providing a reasonable first order approximation (e.g. Schröder et al., 2019, McMillan et al., 2019). The existing approaches to calculating uncertainty are summarised in Table 1 and visualised in Figure 1.

Table 1 – Summary of the existing approaches to calculating uncertainty. Bold highlights aspects where the approach differs between Cryo-TEMPO POCA and Cryo-TEMPO EOLIS.

Step	*Cryo-TEMPO POCA approach*	*Cryo-TEMPO EOLIS approach*
1	Compute a set of elevation differences relative to a reference dataset (ICESat-2)	
2	Compute a grid of **surface slope (and roughness)** based upon an auxiliary dataset	Compute **across-track slope, along-track slope, roughness, power, coherence and distance to POCA** for each measurement
3	Extract co-variates (from step 2) for each elevation difference estimate (from step 1)	
4	Bin elevation differences as a function of extracted co-variates (from step 3)	
5	Compute the **median absolute** elevation difference within each bin, and store as a lookup table	Compute the **upper bound of the confidence interval of the standard deviation** of the elevation difference within each bin, and store as a lookup table
6	Write the uncertainty associated with each POCA elevation measurement based upon the co-variates at the POCA location and the uncertainty value from the lookup table	

To generate a set of elevation differences relative to a reference dataset (Step 1), the effects of temporal changes in surface elevation between the altimetry (CryoSat-2) and reference (ICESat-2) measurements are minimised by restricting the time difference to be less than 1 month in the Cryo-TEMPO POCA approach, and less than 10 days for the Cryo-TEMPO EOLIS approach. A more stringent temporal constraint is applied to the latter owing to the larger amount of data associated with the swath-processed dataset. There is also a requirement that the CryoSat-2 and ICESat-2 measurements are co-located within 20 m of each other (i.e. an order of magnitude less than the CryoSat-2 footprint resolution) for the Cryo-TEMPO POCA approach, in order to minimise any small-scale topographic impact. For the Cryo-TEMPO EOLIS approach, the co-location radius is set to 50 m, and a slope correction is then applied to minimise errors due to variation in topography. Once a set of i elevation difference pairs are identified, a corresponding set of elevation differences is computed:

$$\Delta E_i = E_{POCA,i} - E_{ref,i} \qquad (2)$$

where $E_{POCA,i}$ and $E_{ref,i}$ are the ith pair of CryoSat-2 and ICESat-2 elevations, respectively. These differences combine several factors, including errors in the CryoSat-2 and ICESat-2 measurements and residual differences due to the

https://doi.org/10.5194/egusphere-2026-556
Preprint. Discussion started: 17 March 2026

misalignment of acquisitions in space and time. Owing to the availability of co-located ICESat-2 measurements, elevation differences are available for a subset of CryoSat-2 measurements only, so the elevation differences themselves cannot be used to assign every measurement an associated uncertainty.

Once the set of elevation differences are derived, for each measurement pair, the required co-variate data are extracted, from an auxiliary data file if necessary (Step 3). This information is used to build a look-up table, for each ice sheet, containing estimates of elevation difference binned by each combination of selected co-variates (Step 4). This approach assumes that the uncertainty can be parameterised as a function of the selected co-variates. To derive an uncertainty value for each bin, j, based upon the input elevation difference data, the Cryo-TEMPO POCA approach computes the median absolute difference within each bin (Step 5):

$$\sigma_j = median\left(\left|\Delta E_{i\epsilon j}\right|\right) \quad (3)$$

for all i measurements in slope bin j. This metric captures both the bias and spread of elevation difference measurements relative to the reference dataset within each bin.

For the Cryo-TEMPO EOLIS approach, a different metric is used to derive an uncertainty value for each bin. Instead of the median absolute elevation difference, the standard deviation is calculated from the binned sampled data (Step 5), which provides a measure of the spread, or dispersion, of the elevation differences. To ensure that the sample size in each bin is accounted for, the upper bound of the confidence interval of the standard deviation is calculated:

$$\sigma_j = s\sqrt{\frac{n-1}{\chi^2_{1-a/2}}} \quad (4)$$

where σ_j is standard deviation of the sample, n is sample size, χ^2 is the Chi-square distribution and a is set to 0.05 to give a one-sided 97.5% confidence interval. This upper estimate of the standard deviation is defined as the uncertainty value for each of the bin combinations (Cryo-TEMPO EOLIS, 2024).

If no uncertainty value is available for a given lookup table bin due to the absence of elevation difference data, the bin value is estimated from linear interpolation of the surrounding bins in the Cryo-TEMPO POCA approach, but left unpopulated in the Cryo-TEMPO EOLIS approach. Once the lookup table is constructed, every measurement is assigned an uncertainty based on the lookup table and the co-variate value(s) at its location (Step 6).

https://doi.org/10.5194/egusphere-2026-556
Preprint. Discussion started: 17 March 2026

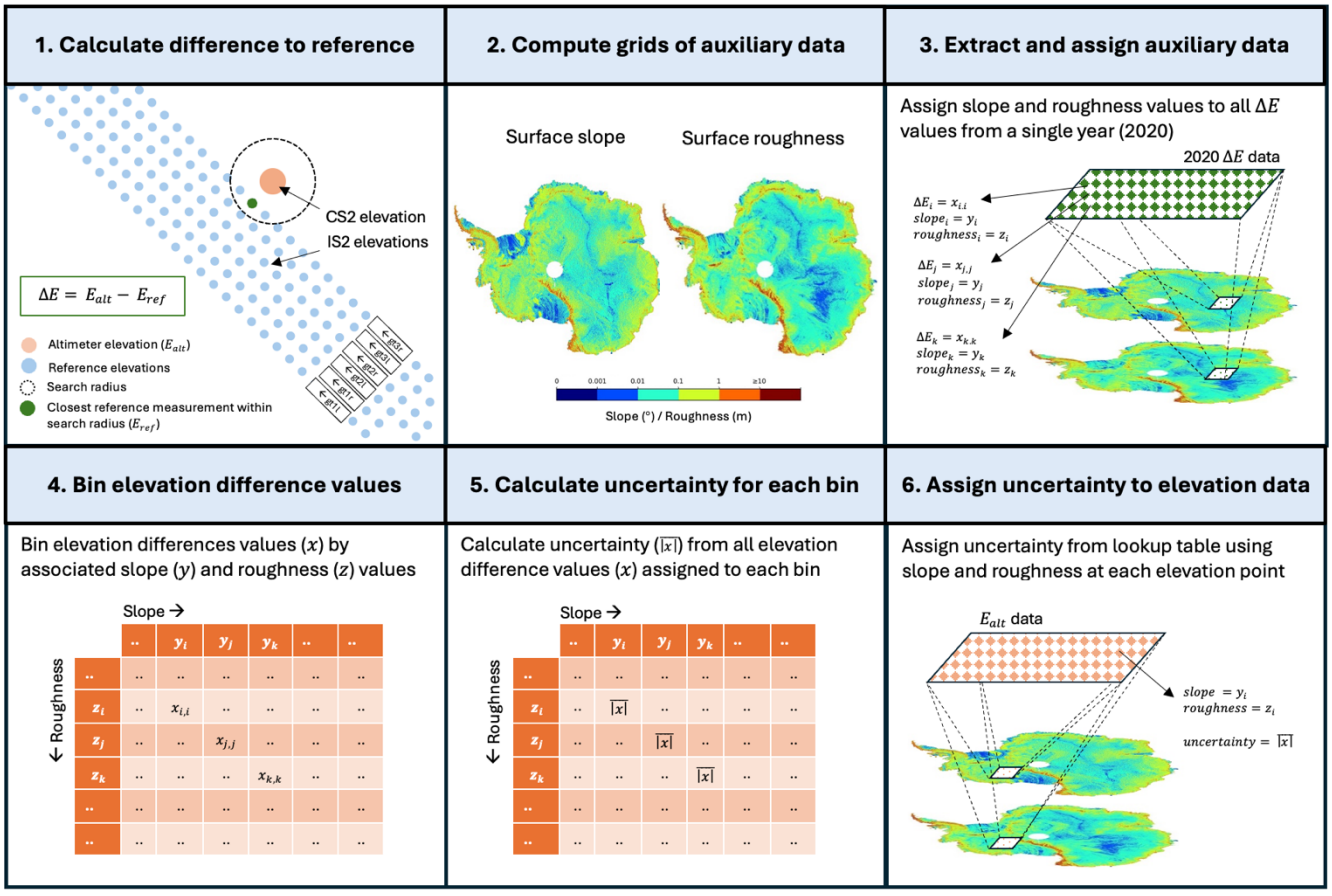

Figure 1 – Uncertainty generation approach taken by Cryo-TEMPO POCA (ESA, 2025b). Boxes correspond to the steps described in Table 1. Approach is conceptually identical to the uncertainty generation approach taken by Cryo-TEMPO EOLIS (ESA, 2019), but the latter uses additional co-variates in Step 2 and a different metric in Step 5.

While these two existing approaches to uncertainty generation are largely comparable in terms of their overall design, two primary differences emerge: first, the choice of co-variates governing the dimensionality of the lookup table (Step 2), and second, the choice of metric used to populate the lookup table (Step 5). In this study, the uncertainty evaluation framework that we develop is thus employed primarily to assess the optimal choice of co-variate(s) and metric when generating both existing (Section 3.2.2) and new (Section 3.2.3) uncertainties.

3.2.2 Inter-comparison and harmonisation of existing methods

To compare, and potentially converge, the differing existing approaches to uncertainty generation (Section 3.2.1), a set of lookup tables are produced and inter-compared using our new uncertainty evaluation framework. The methodologies for ascribing uncertainty values to ice sheet elevation measurements currently differ between the Cryo-TEMPO POCA and

https://doi.org/10.5194/egusphere-2026-556
Preprint. Discussion started: 17 March 2026

Cryo-TEMPO EOLIS approaches both in terms of the number of co-variates used in the generation of the lookup table, and the metric used to populate the lookup table (Table 1). Thus, uncertainties are generated using various co-variate combinations, and three different metrics.

The metrics selected for assessment are the median absolute difference (hereafter median), the upper bound of the confidence interval of the standard deviation (STD UB) and the Root Mean Square Error (RMSE). The median (Equation 3) and STD UB (Equation 4) are selected given their utilisation in the current approach for uncertainty quantification by Cryo-TEMPO POCA and Cryo-TEMPO EOLIS, respectively. RMSE is included, additionally, as a metric that is more sensitive to the influence of outliers in the dataset.

While standardisation in the choice of metric to populate the uncertainty lookup tables associated with both Cryo-TEMPO POCA and Cryo-TEMPO EOLIS is a reasonable aim, such uniformity is less well suited to the choice of co-variates used to build the lookup tables. Some co-variates, for example, such as the distance between POCA and each swath elevation point, are only suitable for use in swath processing. For this reason, the co-variates common to both datasets (i.e. slope, roughness, power and coherence) are used in this analysis.

To further focus the analysis, we consider only combinations of co-variates that best explain the variability observed in the elevation difference dataset. Specifically, correlation coefficients are calculated to determine the statistical relationship between elevation difference and each co-variate by considering the predictive power of each co-variate in isolation. As combining co-variates may further enhance total predictive power, multi-linear regression is also carried out to determine which combination(s) of co-variates are able to best predict elevation difference.

3.2.3 Creation of new uncertainty estimates

To complement our inter-comparison of existing uncertainty generation methods, we also apply our new uncertainty evaluation framework to assess various uncertainties generated for the Sentinel-3 thematic land ice product. In this regard, several co-variate combinations and metrics are evaluated to ascertain their utility in the generation of Sentinel-3 ice sheet elevation uncertainties. Specifically, we evaluate the use of all potential combinations of slope, roughness and power. Coherence is not included here as a potential co-variate as the Sentinel-3 SAR altimeter is not an interferometric instrument. For the reasons stated in Section 3.2.2, we assess the same metrics considered in our CryoSat-2 assessment, namely the median absolute difference (hereafter median), the upper bound of the confidence interval of the standard deviation (STD UB) and the root mean square error (RMSE).

https://doi.org/10.5194/egusphere-2026-556
Preprint. Discussion started: 17 March 2026

4. Results

4.1 Inter-comparison and harmonisation of existing CryoSat-2 uncertainties

First, we present the results of a statistical analysis designed to determine the most favourable combination(s) of co-variates to generate robust uncertainty lookup tables (Section 4.1.1). Next, to assess the robustness of potential CryoSat-2 ice elevation uncertainties and ascertain whether a standardised solution between products is suitable, we show the results of our uncertainty evaluation framework applied to experimental Cryo-TEMPO POCA and Cryo-TEMPO EOLIS ice elevation uncertainty data (Section 4.1.2).

4.1.1 Constraining co-variate combinations

Statistical analysis is carried out to identify the co-variate combinations that best explain the variability observed in the absolute elevation difference to a reference dataset used to generate uncertainties (Section 3.2.1). The correlation coefficients for each individual co-variate show that surface slope has the strongest relationship with the absolute elevation difference, followed by coherence (Table A1; Schröder et al., 2019, McMillan et al., 2019). Multi-linear regression indicates that the highest proportion of variance can be explained when all four co-variates are used, suggesting that each co-variate contributes useful information towards the uncertainty calculation (Table A2). Slope consistently has the most influence on absolute elevation difference as its inclusion within the regression results in R^2 values higher than any combinations that exclude slope. Indeed, slope alone explains a greater proportion of the variance in elevation difference than roughness, power and coherence combined.

Following this initial assessment, we focused our subsequent analysis on the following scenarios: uncertainties generated from lookup tables with all four co-variates; uncertainties generated from lookup tables built with combinations of three co-variates that always include slope; and uncertainties generated from a lookup table with the single best co-variate pair (slope and coherence). In doing so, we assessed the five co-variate combinations that explain the greatest proportion of the absolute elevation difference data in addition to evaluating the value of including more co-variates within the uncertainty models. For each of these combinations, uncertainty lookup tables were generated using each of our three metrics (median, STD UB, RMSE), to allow us to additionally assess the impact of different metric choices. Thus, in total, 15 separate scenarios were evaluated, which are listed in Table A3.

4.1.2 Application of uncertainty evaluation framework

Having determined the set of scenarios to evaluate, we next applied the uncertainty evaluation framework detailed in Section 2 to each scenario, assessing uncertainties computed for both POCA and swath-processed CryoSat-2 data in each case.

https://doi.org/10.5194/egusphere-2026-556
Preprint. Discussion started: 17 March 2026

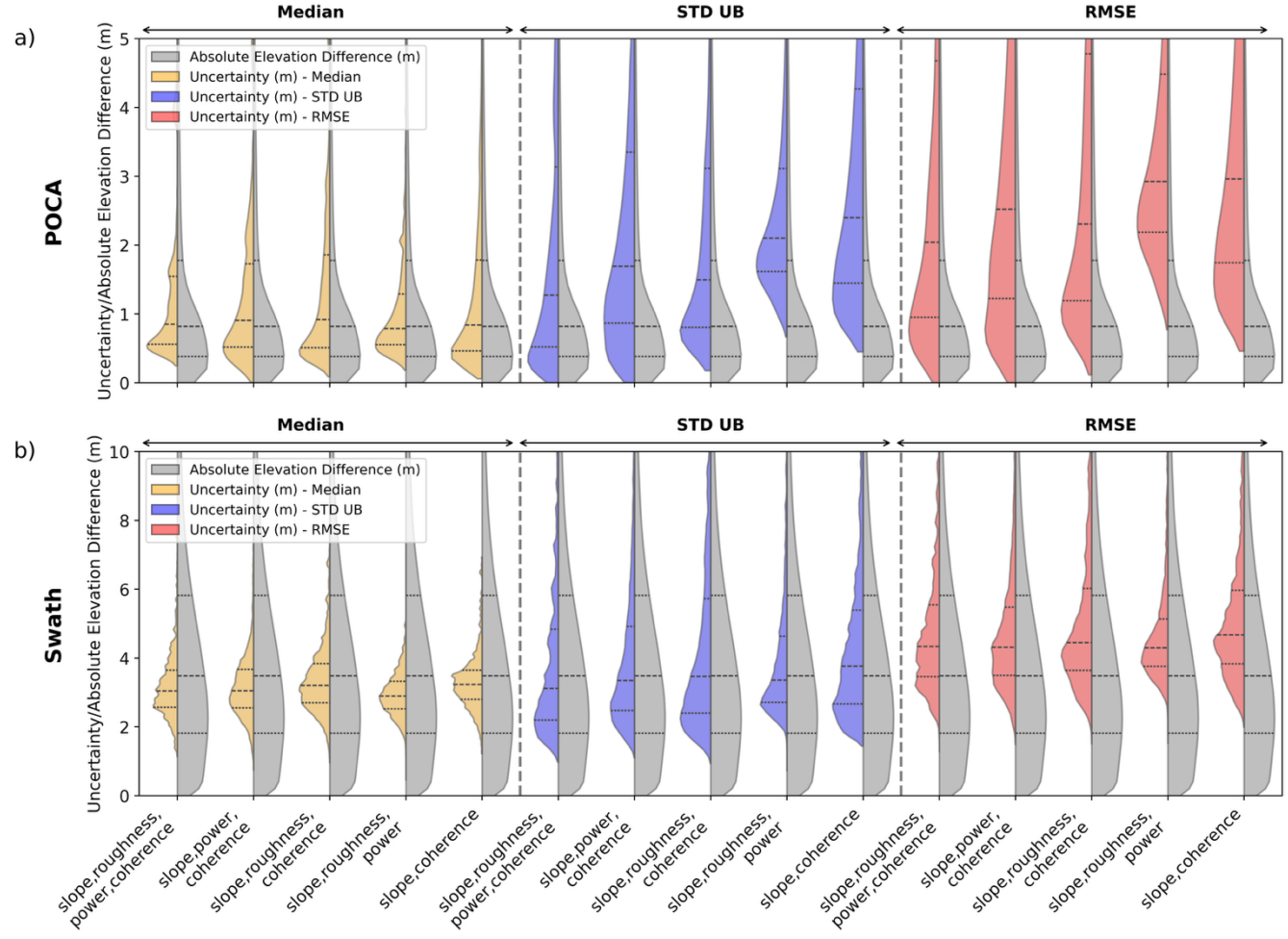

Figure 2 – Comparison of the overall distributions of the absolute elevation differences relative to the reference dataset (grey) and the distribution of uncertainty values calculated using the median (yellow), STD UB (blue) and RMSE (red), for each tested method of uncertainty generation listed in Table A3, for CryoSat-2 **(a)** POCA and **(b)** swath-processed data, over the Antarctic Ice Sheet SARIn region in 2022. Dashed and dotted horizontal black lines denote the median and lower/upper quartiles, respectively, of each distribution.

Figure 2 shows the first component of the uncertainty evaluation framework (Section 2), which compares the overall distribution of uncertainties to the distribution of absolute elevation difference to a reference dataset (hereafter elevation difference), for each of our uncertainty methodologies. Figure 2 suggests that, for both datasets, the choice of metric has a more significant influence on the distribution of uncertainties than the combination of co-variates utilised. Thus, we first discuss the importance of metric choice before considering the choice of co-variates.

https://doi.org/10.5194/egusphere-2026-556
Preprint. Discussion started: 17 March 2026

For the POCA dataset, the median metric results in an uncertainty distribution that aligns most closely with the elevation difference distribution, according to the alignment of the medians and quartiles. The proportion of higher uncertainties (>2 m) generated using STD UB is much greater by comparison, resulting in the uncertainties exhibiting a greater deviation from the distribution of unseen elevation differences in most cases. For the swath dataset, the distribution of elevation differences is much wider than those observed for the POCA dataset. This wider distribution is generally better represented by uncertainties calculated using the STD UB. In both cases, the use of RMSE results in an even greater proportion of high uncertainties (>2 m) such that the distribution of uncertainty values deviates substantially from the distribution of elevation difference values.

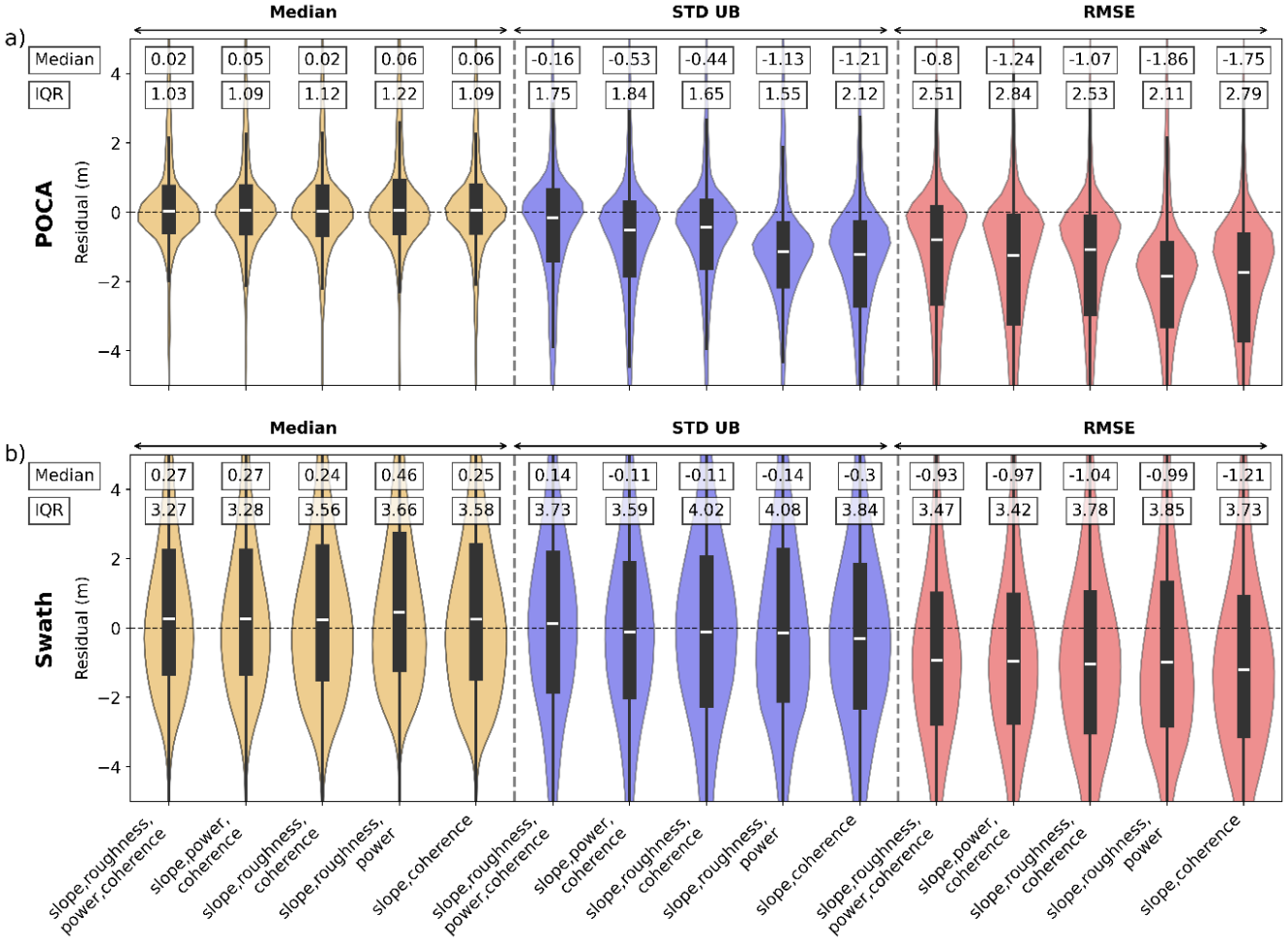

Figure 3 – Comparison of residuals (point-to-point differences between uncertainty and the unseen elevation difference to a reference dataset), for each method of uncertainty generation listed in Table A3, for CryoSat-2 **(a)** POCA and **(b)** swath-processed data, over the Antarctic Ice Sheet SARIn region in 2022. Residual distributions are displayed as violin plots

https://doi.org/10.5194/egusphere-2026-556
Preprint. Discussion started: 17 March 2026

whereby the width represents the proportion of data. Negative (positive) residuals represent cases where the uncertainty is larger (smaller) than the absolute elevation difference. Residual distributions calculated from uncertainties using the median, STD UB and RMSE are coloured yellow, blue and red, respectively. Black box plots are provided within each residual distribution, with a white horizontal line representing the median. The median and inter-quartile range (IQR) are provided for each distribution in text boxes.

The second element of the uncertainty evaluation framework permits analysis of the residuals (i.e. the point-to-point differences between the uncertainty and the elevation difference to an unseen reference dataset) (Figure 3). For the residuals of the POCA dataset, the use of the median metric results consistently in a residual distribution centred most closely to zero (0.02 – 0.06 m), with the narrowest peak, as represented by the smallest IQR (1.03 – 1.22 m). A zero-centred distribution suggests the uncertainty estimates are largely unbiased, while a narrow peak represents a close correspondence between the derived uncertainty and the corresponding observed elevation difference, with ~50% of uncertainty values falling within ~1 m of the elevation difference when the IQR is ~1 m. For the swath dataset, the residuals exhibit less sensitivity with respect to the choice of metric, albeit with the STD UB resulting in generally smaller biases (0.11 – 0.3 m) compared to the median (0.24 – 0.46 m), but the former resulting in a distribution of residuals with a larger IQR (3.59 – 4.02 m) than the latter (3.27 – 3.66 m). Overall, these results indicate that the use of the median as a metric to populate the lookup table results in uncertainty values that correspond most closely overall to the unseen elevation difference values for both datasets, but this choice is less clear for the swath dataset.

The robustness of uncertainties is shown to be further dependent on the chosen co-variates. Regardless of the metric, a reduction in the number of co-variates used to build the uncertainty lookup table typically adversely impacts the uncertainties generated for both the POCA and the swath datasets. This trend is observed both in terms of the divergence of the uncertainty distribution from the elevation difference distribution (Figure 2), and in terms of a shift away from residual distributions with a narrow peak, centred around zero (Figure 3). Specifically, the shift from a four-dimensional to a two-dimensional lookup table typically increases the bias in the residuals. For the POCA uncertainties calculated using the STD UB, for example, a shift in the residual bias from -0.16 to -1.21 m is observed, while a shift from 0.14 to -0.3 m is observed for the swath residuals (Figure 3). The median metric results in a more stable uncertainty solution across all co-variate combinations, particularly for the POCA dataset, although a small shift in the residual bias from 0.02 to 0.06 m is still observed in this case when fewer co-variates are used (Figure 3). Thus, the framework illustrates that granting the uncertainty model more degrees of freedom enables the true accuracy of the data to be better captured.

The cumulative distribution of residuals (Figure 4) demonstrates the proportion of over/under-estimated uncertainties, with the point at which the distribution intersects zero indicating the percentage of negative residuals (where the uncertainty is greater than the recorded elevation difference). The percentage of negative residuals varies according to both the chosen

https://doi.org/10.5194/egusphere-2026-556
Preprint. Discussion started: 17 March 2026

metric, and the combination of co-variates utilised, with the former exhibiting a stronger control. For the POCA data, 60-90% of residuals are negative (indicating over-estimated uncertainties) for uncertainty calculations using STD UB or RMSE, compared to ~50% when the median is used (Figure 4). For the swath data, the similarity between uncertainties generated using the median and the STD UB is clear, with ~45-55% of the data exhibiting a negative residual in both cases, compared to ~65% of the data when the RMSE metric is used (Figure 4). In other words, in terms of the proportion of over/under-estimated uncertainties, the performance of the STD UB metric is more comparable to the performance of the median metric in the swath dataset, than it is for the POCA dataset. Regarding the choice of co-variates, the uncertainty solution for the POCA dataset is most stable across different co-variate combinations when the median metric is selected, whereas for the swath dataset, the choice of co-variates influences the uncertainties, and thus the cumulative distribution of residuals (Figure 4), more significantly.

The cumulative distribution of residuals (Figure 4) also provides information on the overall performance of the residuals, with a steep gradient around zero indicating that a high proportion of uncertainties exhibit close correspondence to the elevation difference. The shallower gradient associated with the swath data (Figure 4) indicates a more dispersed set of residuals suggesting a less close correspondence between uncertainties and elevation differences overall.

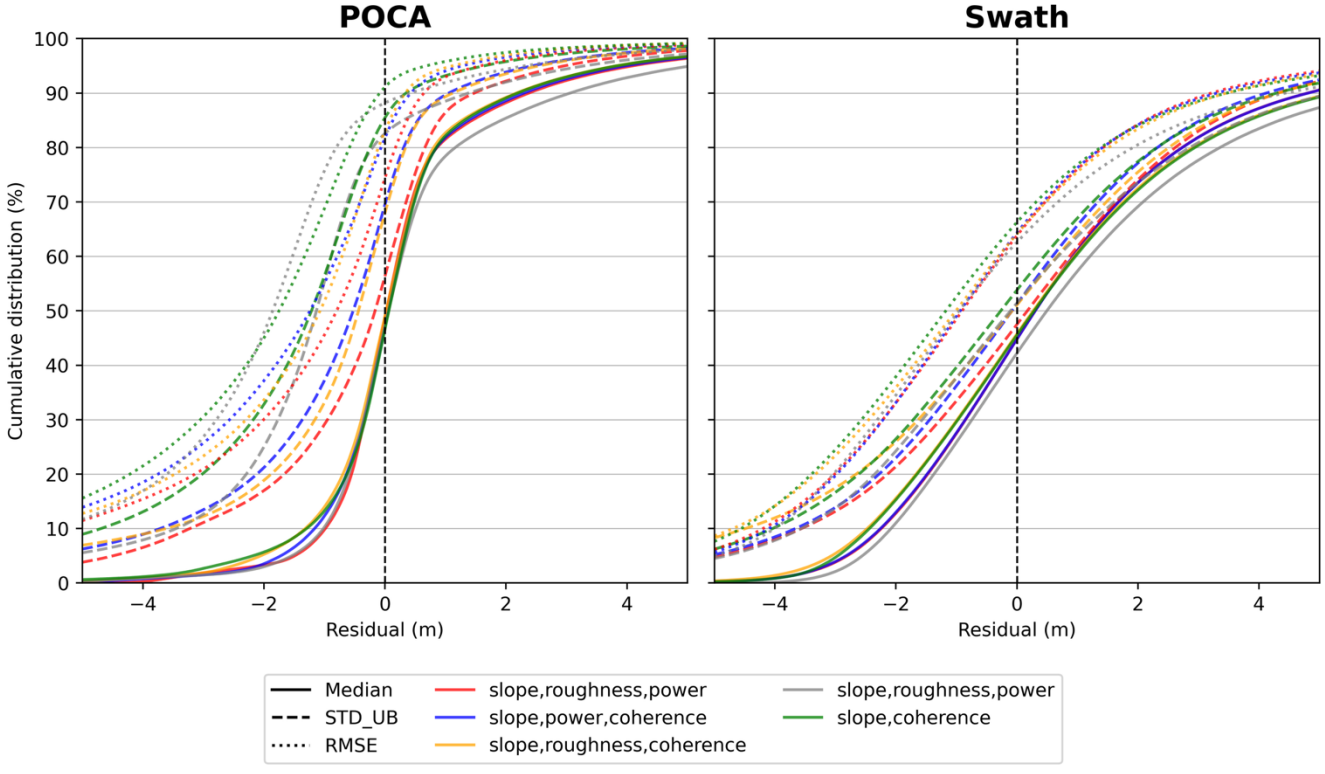

https://doi.org/10.5194/egusphere-2026-556
Preprint. Discussion started: 17 March 2026

Figure 4 – Cumulative distributions of residuals (defined as the difference between the computed uncertainty and the unseen elevation difference relative to ICESat-2 reference dataset), for each method of uncertainty generation for CryoSat-2 POCA (left) and swath-processed (right) data, for the Antarctic Ice Sheet SARIn region in 2022.

Within the previous analysis, we have considered statistics that have been aggregated over the entire coastal region of the ice sheet. Analysis of the spatial distribution of residuals, however, provides information on where regions of under- or over-estimated uncertainties are found. The spatial distribution between under- and over-estimation appears to be relatively random for uncertainties generated using both the median and the STD UB (Figure B3), indicating that there is no tendency for our model to under- or over-estimate uncertainties in regions with specific topographic or climatological characteristics. To complement this, assessing the spatial distribution of the residuals can also serve to identify regions where uncertainty estimates are least accurate, and hence where further improvements to the uncertainty model may provide the greatest gains. For residuals generated from four-dimensional look-up tables using the median or STD UB, for example, values are furthest from zero nearest the coast, indicating that the generation of uncertainty estimates is less accurate in coastal regions (Figure 5), which typically exhibit more complex surface topography and backscattering characteristics.

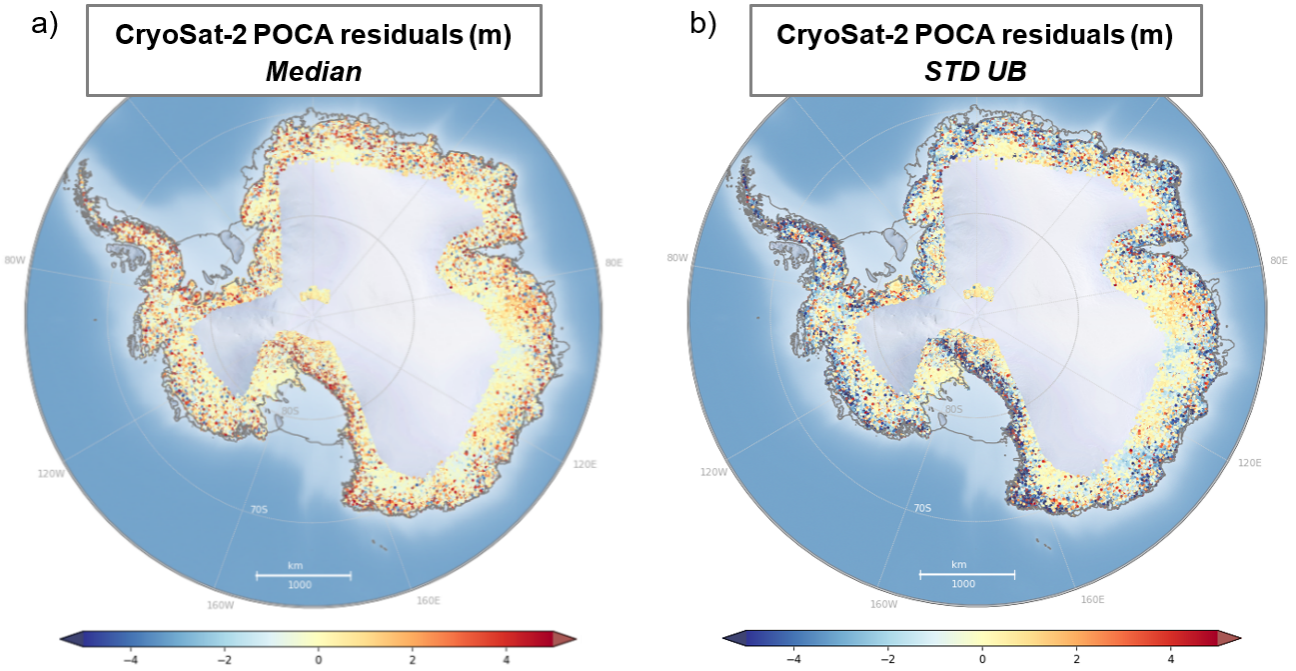

Figure 5 – Map of residuals (the absolute difference relative to reference elevation minus the parameterised uncertainty) for a four-dimensional lookup table, populated using **(a)** median and **(b)** STD UB, for CryoSat-2 POCA data for the Antarctic Ice Sheet SARIn region in 2022. Negative residuals (blue) represent over-estimated uncertainties, and positive residuals (red) represent under-estimated uncertainties.

https://doi.org/10.5194/egusphere-2026-556
Preprint. Discussion started: 17 March 2026

Overall, our uncertainty evaluation framework serves to (1) illuminate the impact of different methodological choices, and (2) identify acceptable solutions for uncertainty generation in Antarctica. For both the POCA and swath-processed CryoSat-2 data, our results show that a higher dimensional lookup table that bins uncertainties according to slope, roughness, power and coherence tends to produce more robust uncertainties than those that are constructed using fewer co-variates. Regarding the choice of metric, our analysis reveals that the use of the median produces the most robust set of uncertainties for the POCA dataset, while the choice between the use of the median and STD UB is less clear for the swath dataset. In the latter case, the use of the median results in a narrower distribution of residuals (Figure 3) indicating a closer point-by-point correspondence between the uncertainties and the unseen elevation difference to a reference dataset. The use of the STD UB, however, yields more conservative uncertainties demonstrated by the higher proportion of negative residuals (Figure 4). For the swath dataset, the choice of metric thus represents a trade-off between most accurately representing the true elevation difference to a reference dataset or generating conservative, over-estimated uncertainties. As such, these results demonstrate how our uncertainty evaluation framework can provide a basis for assessing objectively the validity of uncertainties across different datasets, and for identifying a potential route towards the harmonisation of uncertainty generation across different CryoSat-2 Level-2 ice elevation products.

Next, to assess whether the same conclusions hold when our approach is transferred to a different setting, we apply the same uncertainty evaluation framework to CryoSat-2 data acquired over the Greenland Ice Sheet. The results of this uncertainty evaluation, applied to the same 15 experimental uncertainty generation methods, are shown in Figures B4 - B6. Similar conclusions to those drawn from our Antarctic assessment relating to the benefits of a higher dimensional lookup table also hold for Greenland, with the residual bias being similar or smaller in magnitude when a greater number of co-variates are used to generate the uncertainties (Figure B5). Regarding the choice of metric, the median metric results in an uncertainty solution that is similar across all co-variate combinations (i.e. most stable), as was the case for Antarctica. For the four-dimensional POCA lookup table, central and narrow residual distributions are generated using both the median (median=0.01 m, IQR=1.43 m) and the STD UB (median=-0.11 m, IQR=1.52 m). For the swath data, it is clear that the median results in a more desirable set of residuals (median=0.18 m, IQR=2.0) compared to those produced using the STD UB (median=-0.71 m, IQR=2.29 m). The choice of metric for the swath dataset is thus more clear in Greenland than it is for Antarctica. Such results demonstrate the ability of the uncertainty evaluation framework to resolve subtle differences in uncertainty robustness according to the region of interest and Level-2 processing applied.

4.2 Creation of new uncertainty estimates for Sentinel-3

We apply our uncertainty evaluation framework (Section 2) to uncertainties created for Sentinel-3 ice sheet elevation data to demonstrate its ability to inform the construction of new uncertainty parameters for missions that are currently lacking such information. More specifically, the uncertainty evaluation framework is used to assess 12 possible methods for generating

https://doi.org/10.5194/egusphere-2026-556
Preprint. Discussion started: 17 March 2026

uncertainties for Sentinel-3 data (Table A4). In this case, all available co-variate combinations are tested, negating the requirement for statistical analysis to determine the most promising co-variate combinations.

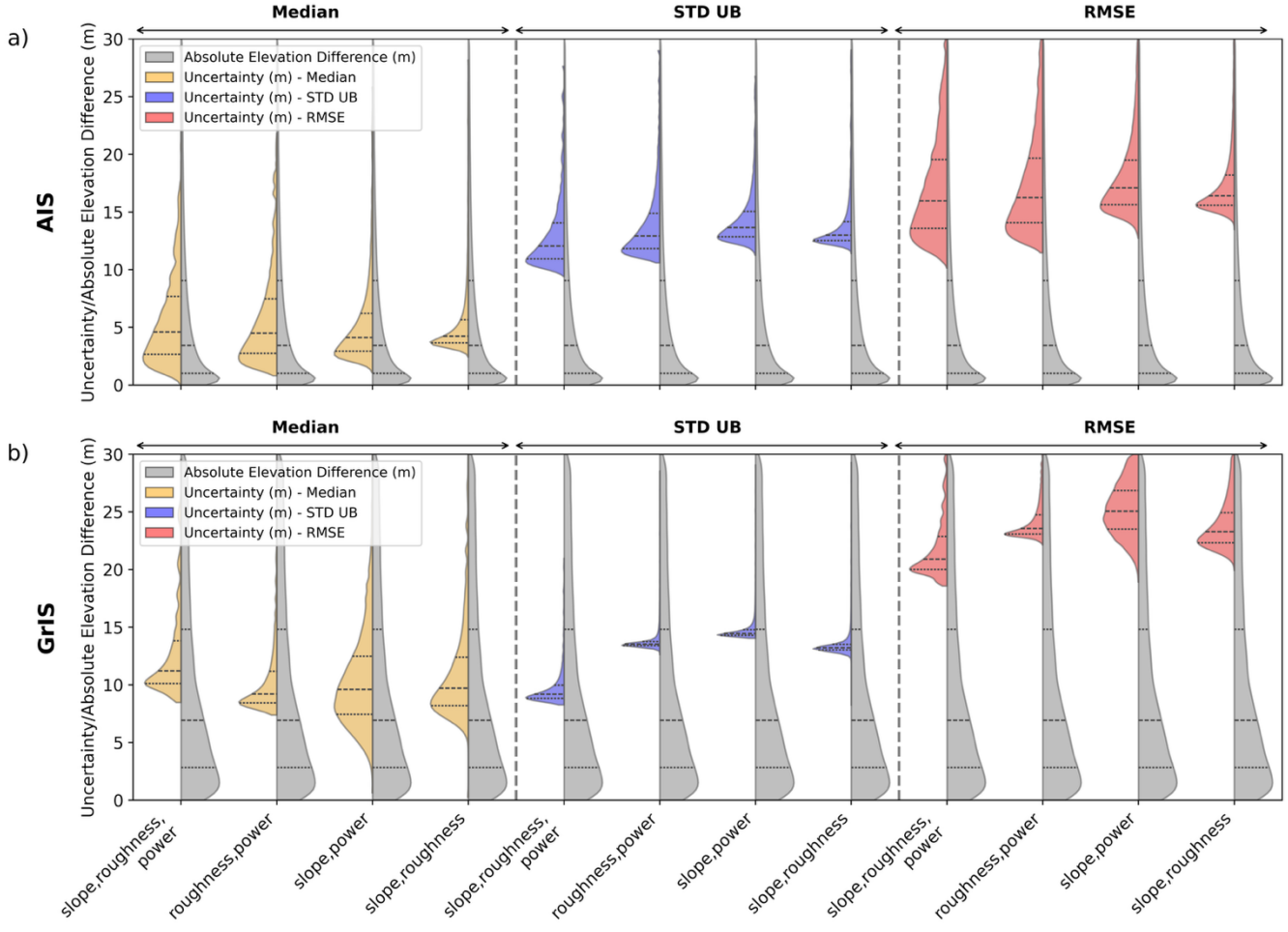

415 **Figure 6** – Comparison of the overall distributions of the absolute elevation differences relative to the reference dataset (grey) and the distribution of uncertainty values calculated using the median (yellow), STD UB (blue) and RMSE (red), for each tested method of uncertainty generation listed in Table A4, for Sentinel-3 thematic data, over the **(a)** Antarctic Ice Sheet (AIS) and **(b)** Greenland Ice Sheet (GrIS) in 2022. Dashed and dotted horizontal black lines denote the median and lower/upper quartiles, respectively, of each distribution.

420

The results of the first component of the uncertainty evaluation framework (Figure 6) show that the distribution of uncertainties is sensitive to both the choice of metric and co-variates. Good agreement between the distribution of uncertainty and elevation difference is observed in Antarctica when the median is the chosen metric, but agreement is

https://doi.org/10.5194/egusphere-2026-556
Preprint. Discussion started: 17 March 2026

degraded significantly by other solutions. The ability of the uncertainty distribution to represent the elevation difference distribution is further degraded when the analysis is performed for data acquired over Greenland. There, in most cases, the uncertainties do not adequately capture the tails of the elevation difference distribution, which are much larger than for CryoSat-2 (Figure 2) whose design is more optimised for the measurement of ice surfaces.

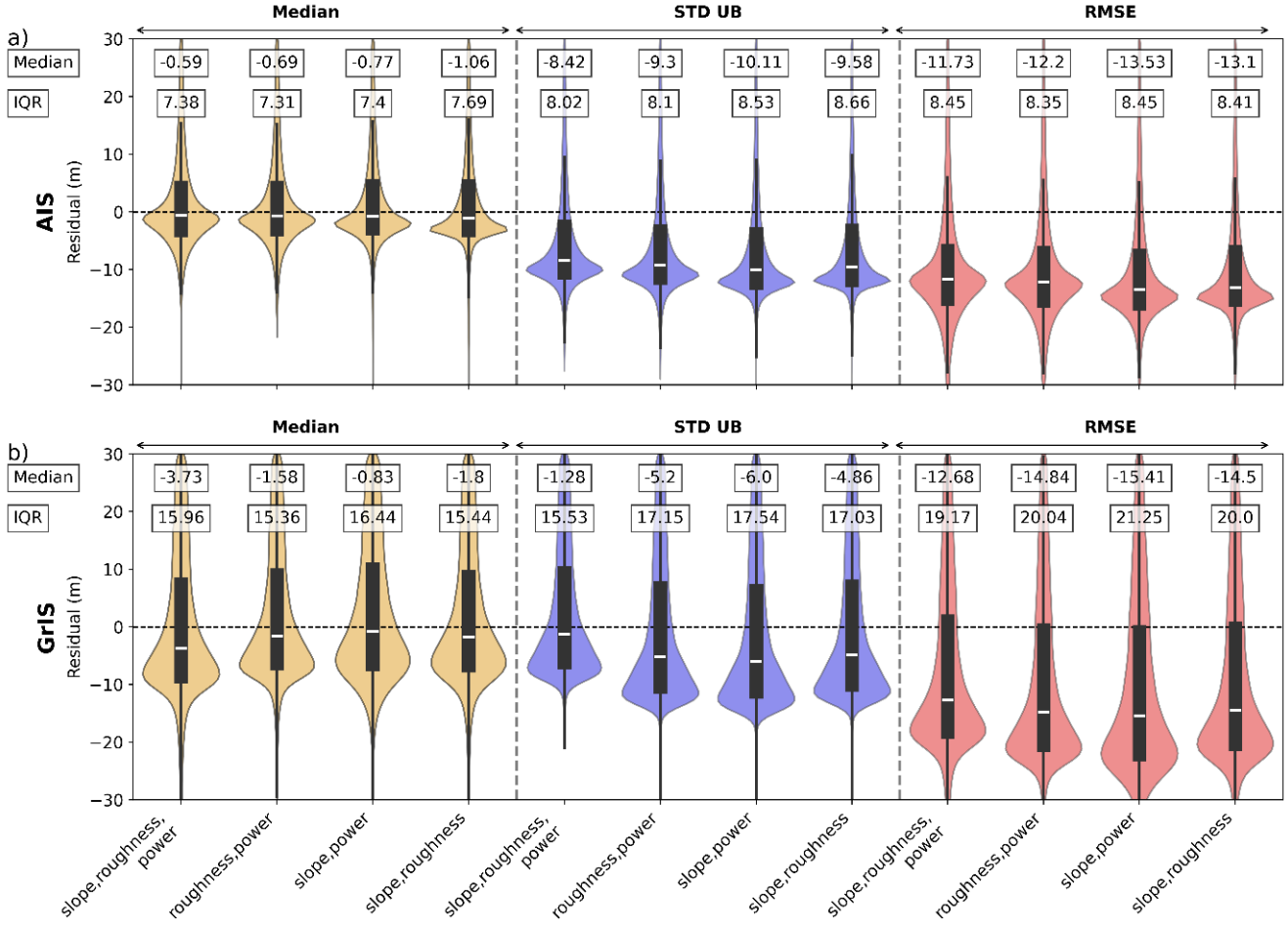

Figure 7 – Comparison of residuals (difference between uncertainty and the unseen elevation difference to a reference dataset), for each method of uncertainty generation listed in Table A4, for Sentinel-3 thematic data over the **(a)** Antarctic Ice Sheet (AIS) and **(b)** Greenland Ice Sheet (GrIS) in 2022. Residual distributions are displayed as violin plots whereby the width represents the proportion of data. Negative (positive) residuals represent cases where the uncertainty is larger (smaller) than the absolute elevation difference. Residual distributions calculated from uncertainties using the median, STD UB and RMSE are coloured yellow, blue and red, respectively. Black box plots are provided within each residual distribution, with a

https://doi.org/10.5194/egusphere-2026-556
Preprint. Discussion started: 17 March 2026

white horizontal line representing the median. The median and inter-quartile range (IQR) are provided for each distribution in text boxes.

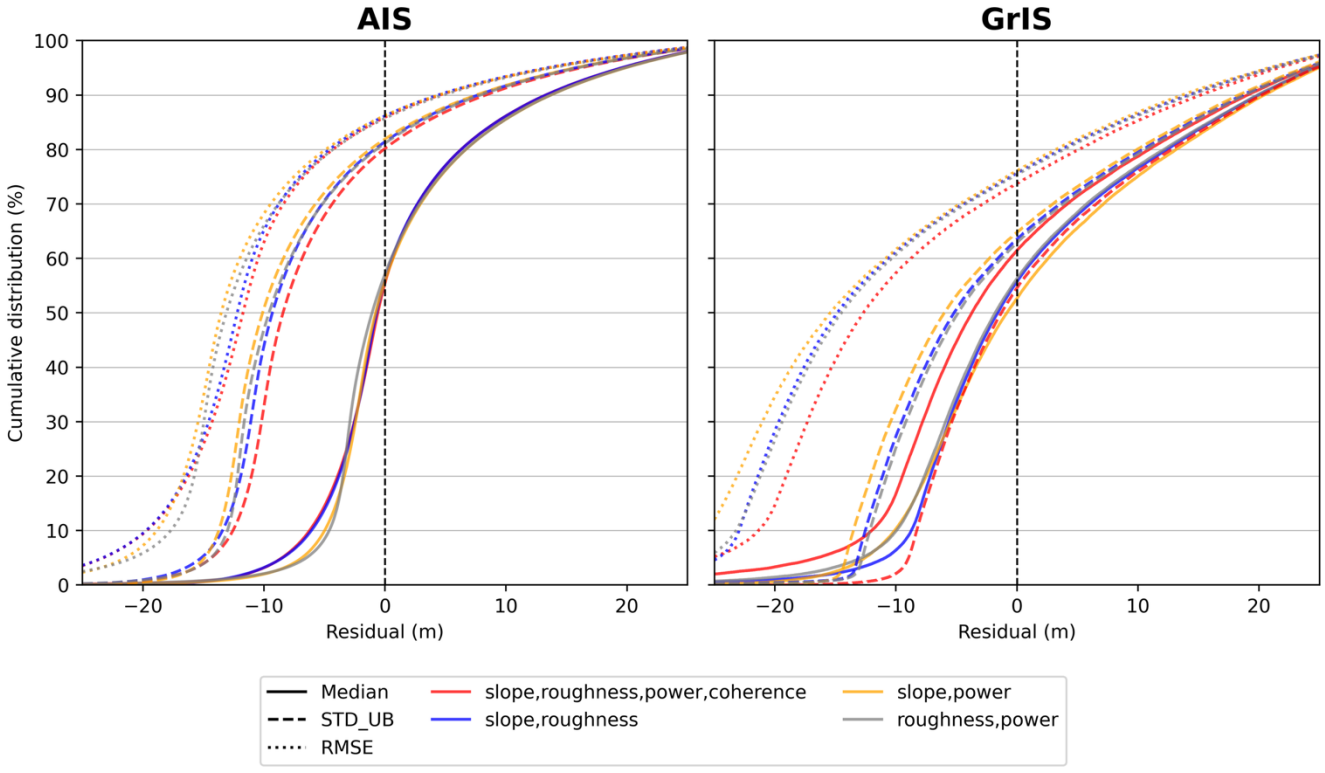

Figure 8 – Cumulative distributions of residuals (difference between uncertainty and the unseen elevation difference relative to a reference dataset), for each method of uncertainty generation for Sentinel-3 thematic data, for the Antarctic Ice Sheet (left) and the Greenland Ice Sheet (right) in 2022.

The distributions and cumulative distributions of the residuals, displayed in Figures 7 and 8, respectively, and comprising the second component of the uncertainty evaluation framework, show that, for the Antarctic Ice Sheet, the choice of metric significantly influences the robustness of uncertainties generated. Despite the relative consistency between metrics in terms of the IQR of the residuals (~8 m), the use of the median metric consistently results in a distribution of residuals centred around 1 m, whereas the other two metrics result in a bias exceeding ~10 m in magnitude (Figure 7). As a result, the use of the STD UB or RMSE metrics result in 80-90% of uncertainties being over-estimated (Figure 8).

The spread of residuals is greater over Greenland than over Antarctica (Figure 7) owing to the narrower distribution of uncertainties generated, which fails to capture the true spread in elevation differences (Figure 6). The metric-driven differences in uncertainties are similar to those in Antarctica in that the residual bias is generally smallest when the median

https://doi.org/10.5194/egusphere-2026-556
Preprint. Discussion started: 17 March 2026

metric (~2 m) is used, compared to the STD UB (~5 m) or RMSE (~14 m). In terms of the percentage of negative residuals (where the uncertainty is greater than the recorded elevation difference), the distinction between the median and the STD UB is less clear in Greenland than in Antarctica, as seen by the overlapping cumulative distributions (Figure 8). In Greenland, when STD UB is used, ~55-65% of residuals are negative compared to ~80% in Antarctica, corresponding to a lesser tendency for STD UB to over-estimate uncertainties in Greenland. Importantly, as demonstrated here, our uncertainty evaluation framework provides an objective and systematic mechanism to identify and assess these subtle differences in the robustness and interpretation of Sentinel-3 uncertainties, which have been generated for the first time across both the Antarctic and Greenland ice sheets.

5. Discussion

We have demonstrated the capability of our new framework to assess the robustness of uncertainties generated for radar altimeter-derived ice sheet elevation measurements. The framework has been applied to assess both existing (Section 4.1) and new (Section 4.2) uncertainty generation approaches, across both ice sheets, for the CryoSat-2 and Sentinel-3 missions, respectively. We provide demonstrable evidence in each case for the differences in the uncertainty robustness (i.e. performance) that can arise from the choice of metric or co-variates; knowledge that, until now, has been lacking. Overall, our results show that the median metric applied to a higher dimensional lookup table typically produces the most robust set of uncertainties. The relative merits of alternative solutions, however, are shown to be contingent upon the Level-2 processing (Section 5.1), satellite source (Section 5.2) and ice sheet (Section 5.3). Potential explanations for these variations in performance are discussed next.

5.1 Level-2-processing-driven variability in uncertainty generation

The inter-comparison of uncertainty generation methods for POCA and swath-processed CryoSat-2 ice elevation data provides the basis for improved harmonisation between existing approaches as high-dimensional lookup tables populated using the median metric are shown to produce robust uncertainties for both datasets. The optimal choice of metric is less clear, however, depending on the Level-2 processing applied. Specifically, for swath-processed data in Antarctica, our analysis indicates that the benefits of the median over the STD UB are less clear than for the POCA dataset (Figure 3). Swath-processed data retrieves ice sheet elevation measurements from multiple locations across the satellite swath (Gourmelen et al., 2018), and has, on average, a lower accuracy than the POCA dataset, which retrieves ice sheet elevation only at the point of closest approach to the satellite (Wingham et al., 2006b). For this reason, the spread of absolute elevation differences assigned to each co-variate bin (Step 4, Table 1) is greater for the swath-processed dataset. By definition, these outliers are captured more explicitly by the STD UB metric than by the median, thus providing a potential explanation as to why the more conservative uncertainties generated using the STD UB may comprise a more representative solution for swath-processed data.

https://doi.org/10.5194/egusphere-2026-556
Preprint. Discussion started: 17 March 2026

5.2 Satellite-driven variability in uncertainty generation

Moving beyond the single satellite case, the standardised nature of the framework also enables the systematic inter-comparison of uncertainties between different satellites; in this case demonstrated by the inter-comparison of uncertainties associated with CryoSat-2 and Sentinel-3.

The results derived from the uncertainty evaluation framework clearly illustrate the inferior performance of the uncertainties generated for Sentinel-3, compared to those derived for CryoSat-2 ice elevation data. Notably, a greater deviance between the uncertainty distribution and the distribution of unseen elevation difference data is observed for Sentinel-3 (Figure 6) than for CryoSat-2 (Figure 2), and the residual bias (i.e. a measure of the representativeness of a given uncertainty estimate) is on the scale of metres (Figure 7) rather than centimetres (Figure 3). The inter-satellite assessment enabled by our framework shows that the Sentinel-3 uncertainties do not replicate the accuracy captured by the CryoSat-2 uncertainties, but instead significantly over-estimate the observed elevation difference to a reference dataset. As such, the framework aids understanding of the generated values for Sentinel-3 as maximum possible uncertainties, which is key for the effective interpretation and application of these new uncertainties by potential users.

The framework also reveals the greater variability between potential uncertainty solutions for Sentinel-3 compared to CryoSat-2. Owing to the non-interferometric nature of Sentinel-3 and its smaller range window relative to CryoSat-2 (McMillan et al., 2019), a broader distribution of elevation differences relative to the reference data, including a greater proportion of outliers, is expected compared to CryoSat-2. As such, metrics that are more sensitive to the presence of outliers, such as STD UB and RMSE, are likely to produce uncertainty solutions that deviate greatly from those calculated using the median; more so than can be expected for datasets with a lower proportion of outliers, such as those associated with CryoSat-2.

Overall, the application of a standardised framework across different radar altimeters (CryoSat-2 and Sentinel-3) provides a systematic process for making quantitative and robust assessments of the relative accuracies of uncertainties between different satellite missions. Ultimately, the framework suggests that our first-pass Sentinel-3 uncertainties are less accurate than those derived for CryoSat-2, and thus motivate and direct future work to further refine the metrics and/or co-variates used in Sentinel-3 uncertainty generation.

5.3 Regional variability in uncertainty generation

Application of the uncertainty evaluation framework to both CryoSat-2 and Sentinel-3 data demonstrated that the performance of uncertainties differs between Antarctica and Greenland. In Antarctica, the use of the median metric produces a more zero-centred and narrower distribution of residuals (Figures 3 and 7), representing a closer agreement between

https://doi.org/10.5194/egusphere-2026-556
Preprint. Discussion started: 17 March 2026

uncertainty values and the unseen elevation differences relative to the reference dataset. In contrast, the STD UB metric results typically in an overly conservative set of uncertainty estimates. For Greenland, however, the advantages of the use of the median are less clear in some cases. For CryoSat-2 POCA data, for example, the STD UB can result in a similar set of uncertainties (Figure B4) and residuals (Figure B5) to those generated using the median metric.

The different levels of confidence in the optimal uncertainty generation approach between Antarctica and Greenland may be explained by the differing data volumes and topographical complexity associated with each region. Due to its size and latitudinal extent, a smaller number of elevation retrievals are acquired over Greenland, compared to Antarctica, resulting in a lower number of elevation difference values being assigned to each bin during the uncertainty lookup table construction (Step 4, Table 1). Moreover, the median ice sheet surface slope and roughness are approximately 2.5 times greater for Greenland than Antarctica (Figure B2; Phillips and McMillan, 2024). The enhanced topographical complexity of Greenland likely degrades the quality of altimetry measurements (Bamber et al., 1998; Brenner et al., 2007; McMillan et al., 2019), resulting in a broader distribution of elevation difference values within each bin. Owing to both the smaller total number of data points and the lower quality of these data, the variability of elevation difference data within each bin is greater in Greenland, with a greater proportion of outlier values (Figure B7). The median metric is unlikely to capture such pervasive outliers, implying that its performance may not be as robust in regions, such as Greenland, where the distribution of elevation differences is less Gaussian in nature.

Ultimately, our uncertainty evaluation framework has demonstrated proficiency in distinguishing subtle differences in uncertainty robustness between Antarctica and Greenland. For Antarctica, where the data volume is greater and the topographical complexity is lower, the median provides a robust solution for uncertainties. The results of the framework suggest that the benefits of this approach, however, are less clear for Greenland, where data volume is smaller and topographical complexity is greater.

6. Summary and implications

We have developed a novel framework to systematically assess the performance of existing and evolving uncertainties generated for altimetry-based ice sheet elevation measurements. By using this framework to compare a range of uncertainty generation approaches for POCA and swath-processed CryoSat-2 ice sheet elevation data, we have demonstrated how uncertainty calculation can be assessed and standardised between products. Exploitation of the framework has also enabled the development of a set of uncertainties for Sentinel-3 ice sheet elevation data, for the first time, and aided their interpretation as an initial set of maximum uncertainties. Importantly, our framework has identified that the median metric applied to a higher dimensional lookup table often produces the most robust set of uncertainties, but the Level-2 processing,

https://doi.org/10.5194/egusphere-2026-556
Preprint. Discussion started: 17 March 2026

satellite source and ice sheet can each affect the robustness of uncertainties generated. Such findings can help to guide principal avenues for future research to improve radar-altimeter-derived ice sheet elevation uncertainties.

Overall, our framework represents an important foundation for the systematic production and characterisation of uncertainties across all ice sheet altimetry measurements, spanning the full collection of past, current and future altimeter missions. Moreover, as the framework is agnostic to the method of uncertainty computation, it can also be used in the future to compare the performance of current empirical approaches with newly developed methods, such as those based on the formal propagation of errors from Level 0 or 1. The framework could also be applied beyond the life span of ICESat-2 should alternative suitable reference data exist, such as from dedicated airborne campaigns. The evaluation of ice sheet altimetry uncertainty estimates in this way is required for a wide range of scientific and operational applications. More specifically, this new framework can play a key role in optimising uncertainties associated with upcoming polar radar altimetry missions, such as the Copernicus Polar Ice and Snow Topography Altimeter (CRISTAL) and the Sentinel-3 Next Generation Topography mission, and in combining these data with observations from other coincident missions, such as the existing Copernicus Sentinel-3 constellation. Ultimately, a consistent and well-validated approach to uncertainty estimation is an essential component of combining measurements from multiple missions, which in turn will enable more refined estimations of ice sheet mass loss contributions to global sea-level rise, and help to facilitate the use of satellite altimeter observations in the development and validation of numerical ice sheet projections.

https://doi.org/10.5194/egusphere-2026-556
Preprint. Discussion started: 17 March 2026

Appendices

Appendix A

Table A1 – Correlation coefficients of absolute elevation difference with each co-variate

Co-variate	***R***
Slope	0.324
Roughness	0.277
Power	-0.218
Coherence	-0.285

Table A2 – Multi-linear regression between absolute elevation difference and all co-variate combinations, ordered from higher to lower predictive power (i.e. R^2 value)

Co-variate				***R^2***
Slope	Roughness	Power	Coherence	0.196
Slope	Roughness	-	Coherence	0.196
Slope	-	Power	Coherence	0.194
Slope	-	-	Coherence	0.194
Slope	Roughness	Power	-	0.193
Slope	-	Power	-	0.189
Slope	Roughness	-	-	0.168
Slope	-	-	-	0.167
-	Roughness	Power	Coherence	0.162
-	Roughness		Coherence	0.162
-	Roughness	Power	-	0.152
-	Roughness	-	-	0.110
-	-	Power	Coherence	0.099
-	-	-	Coherence	0.087
-	-	Power	-	0.039

https://doi.org/10.5194/egusphere-2026-556
Preprint. Discussion started: 17 March 2026

Table A3 – List of parameters included for each CryoSat-2 uncertainty estimation scenario

Metric	***Number of co-variates***	***Co-variate combination***			
Median	4 co-variates	Slope	Roughness	Power	Coherence
	3 co-variates	Slope	-	Power	Coherence
		Slope	Roughness	-	Coherence
		Slope	Roughness	Power	-
	2 co-variates	Slope	-	-	Coherence
STD UB	4 co-variates	Slope	Roughness	Power	Coherence
	3 co-variates	Slope	-	Power	Coherence
		Slope	Roughness	-	Coherence
		Slope	Roughness	Power	-
	2 co-variates	Slope	-	-	Coherence
RMSE	4 co-variates	Slope	Roughness	Power	Coherence
	3 co-variates	Slope	-	Power	Coherence
		Slope	Roughness	-	Coherence
		Slope	Roughness	Power	-
	2 co-variates	Slope	-	-	Coherence

575

Table A4 – List of parameters included for each Sentinel-3 uncertainty estimation scenario

Metric	***Number of co-variates***	***Co-variate combination***		
Median	3 co-variates	Slope	Roughness	Power
	2 co-variates	-	Roughness	Power
		Slope	-	Power
		Slope	Roughness	-
STD UB	3 co-variates	Slope	Roughness	Power
	2 co-variates	-	Roughness	Power
		Slope	-	Power
		Slope	Roughness	-
RMSE	3 co-variates	Slope	Roughness	Power
	2 co-variates	-	Roughness	Power
		Slope	-	Power
		Slope	Roughness	-

https://doi.org/10.5194/egusphere-2026-556
Preprint. Discussion started: 17 March 2026

Appendix B

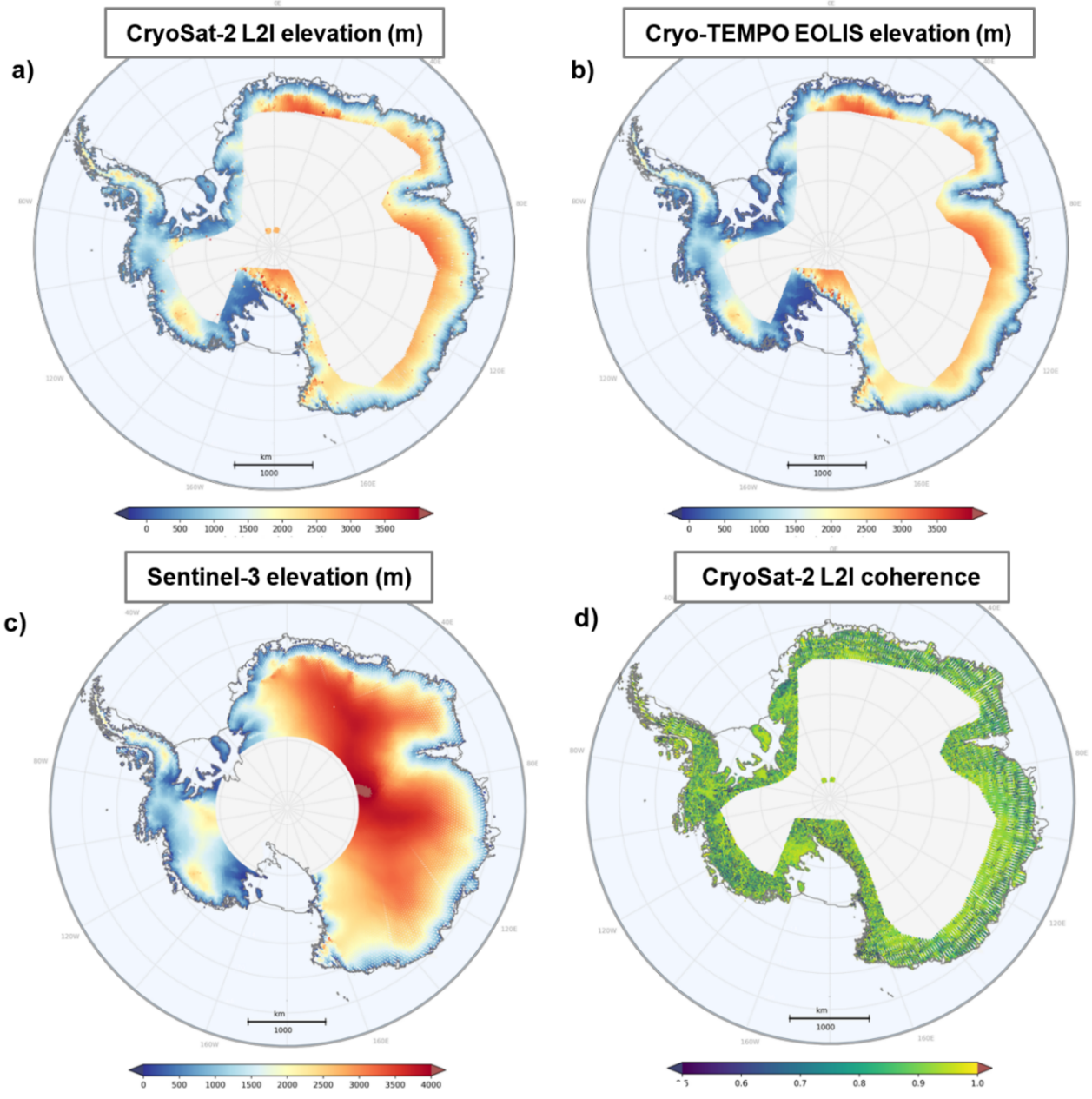

https://doi.org/10.5194/egusphere-2026-556
Preprint. Discussion started: 17 March 2026

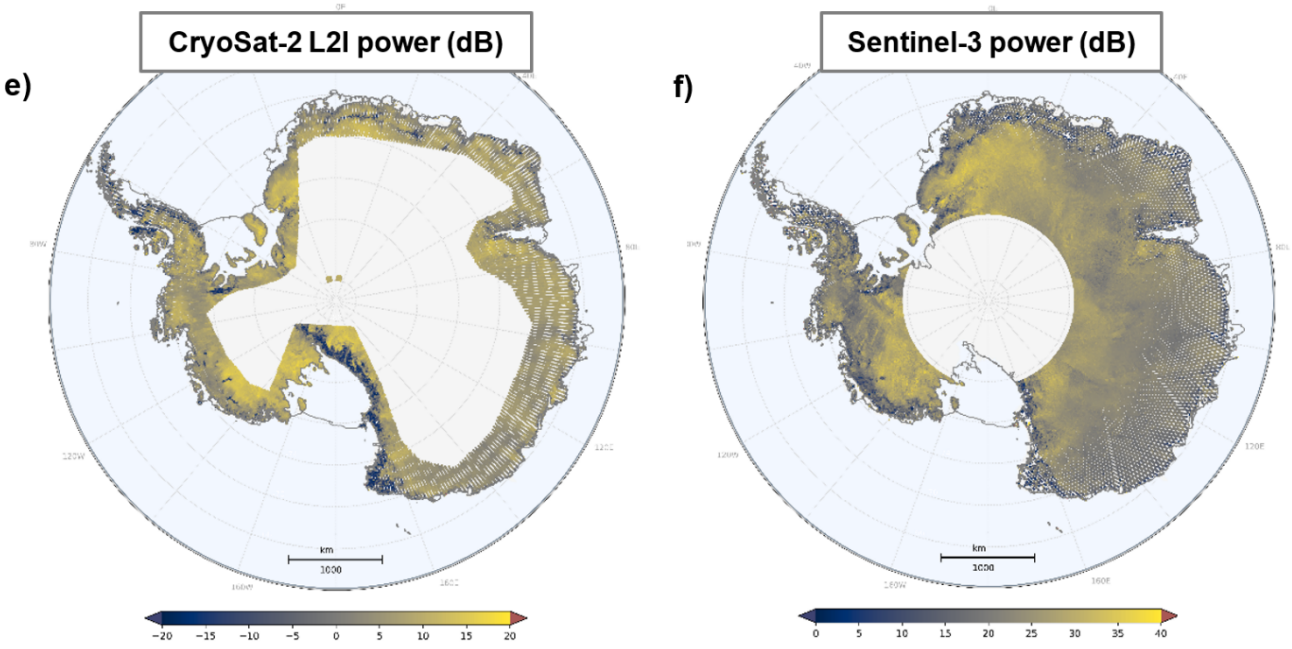

Figure B1 – Data used in uncertainty calculations over the Antarctic Ice Sheet. **(a)** CryoSat-2 L2I POCA elevation; **(b)** Cryo-TEMPO EOLIS elevation; **(c)** Sentinel-3 Hydro-Cryo Thematic Product elevation; **(d)** CryoSat-2 L2I POCA coherence; **(e)** CryoSat-2 L2I POCA power; **(f)** Sentinel-3 Hydro-Cryo Thematic Product power.

585

https://doi.org/10.5194/egusphere-2026-556
Preprint. Discussion started: 17 March 2026

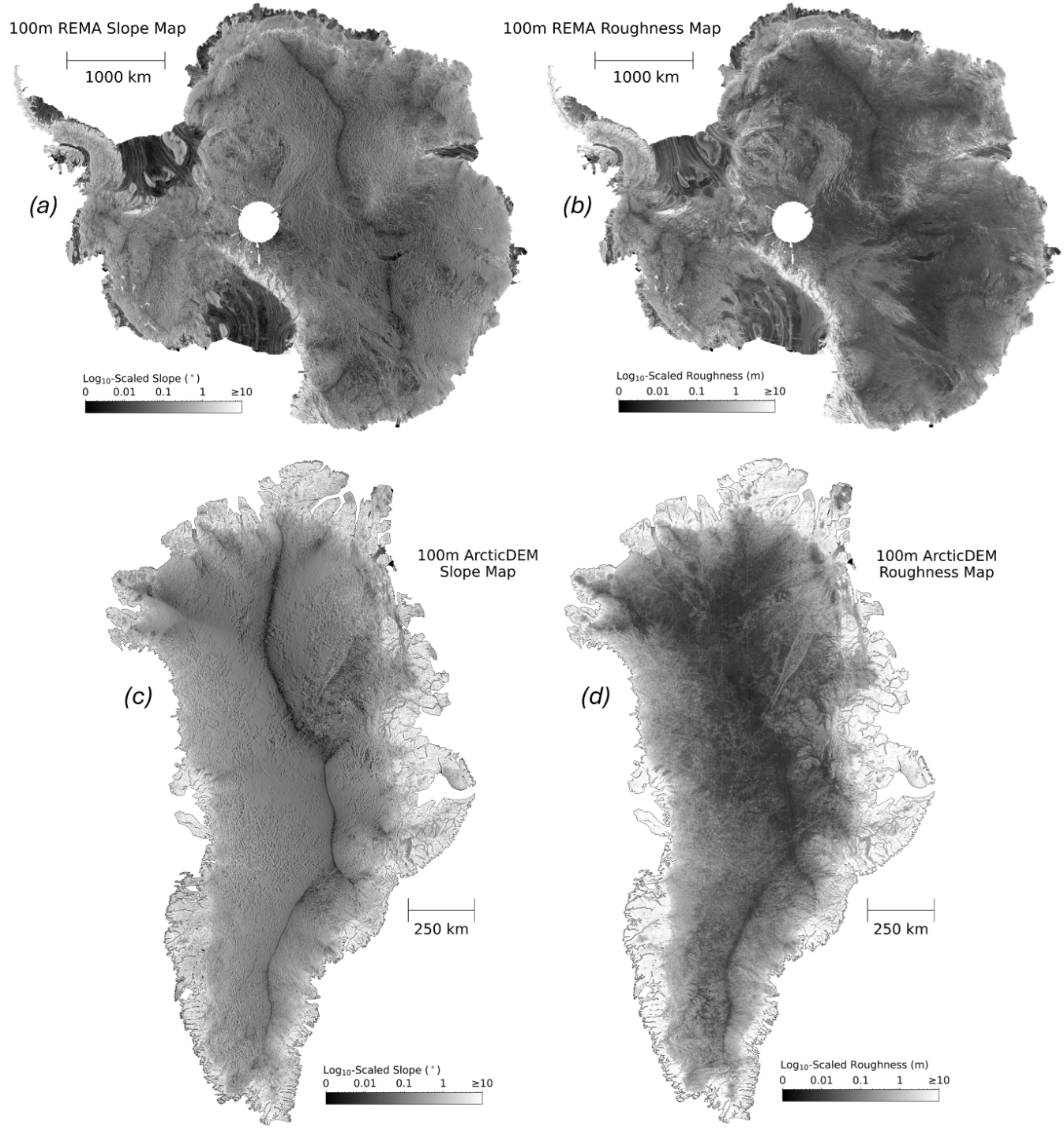

Figure B2 – Surface slope **(a, c)** and surface roughness **(b, d)** data used in uncertainty calculations over the Antarctic Ice Sheet **(a-b)** and the Greenland Ice Sheet **(c-d)**.

https://doi.org/10.5194/egusphere-2026-556
Preprint. Discussion started: 17 March 2026

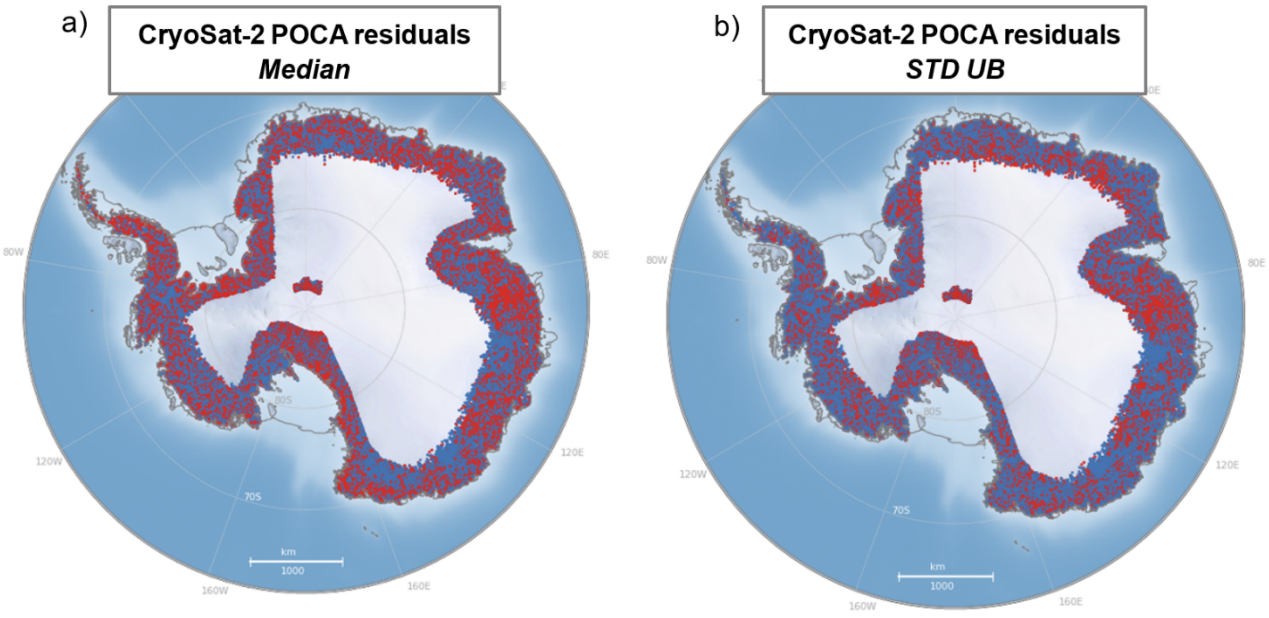

590

Figure B3 – Map of negative (blue) and positive (red) residuals (the absolute difference relative to reference elevation minus the parameterised uncertainty) for a four-dimensional lookup table, populated using **(a)** median and **(b)** STD UB, for CryoSat-2 POCA data for the Antarctic Ice Sheet SARIn region in 2022. Negative residuals (blue) represent over-estimated uncertainties, and positive residuals (red) represent under-estimated uncertainties.

595

https://doi.org/10.5194/egusphere-2026-556
Preprint. Discussion started: 17 March 2026

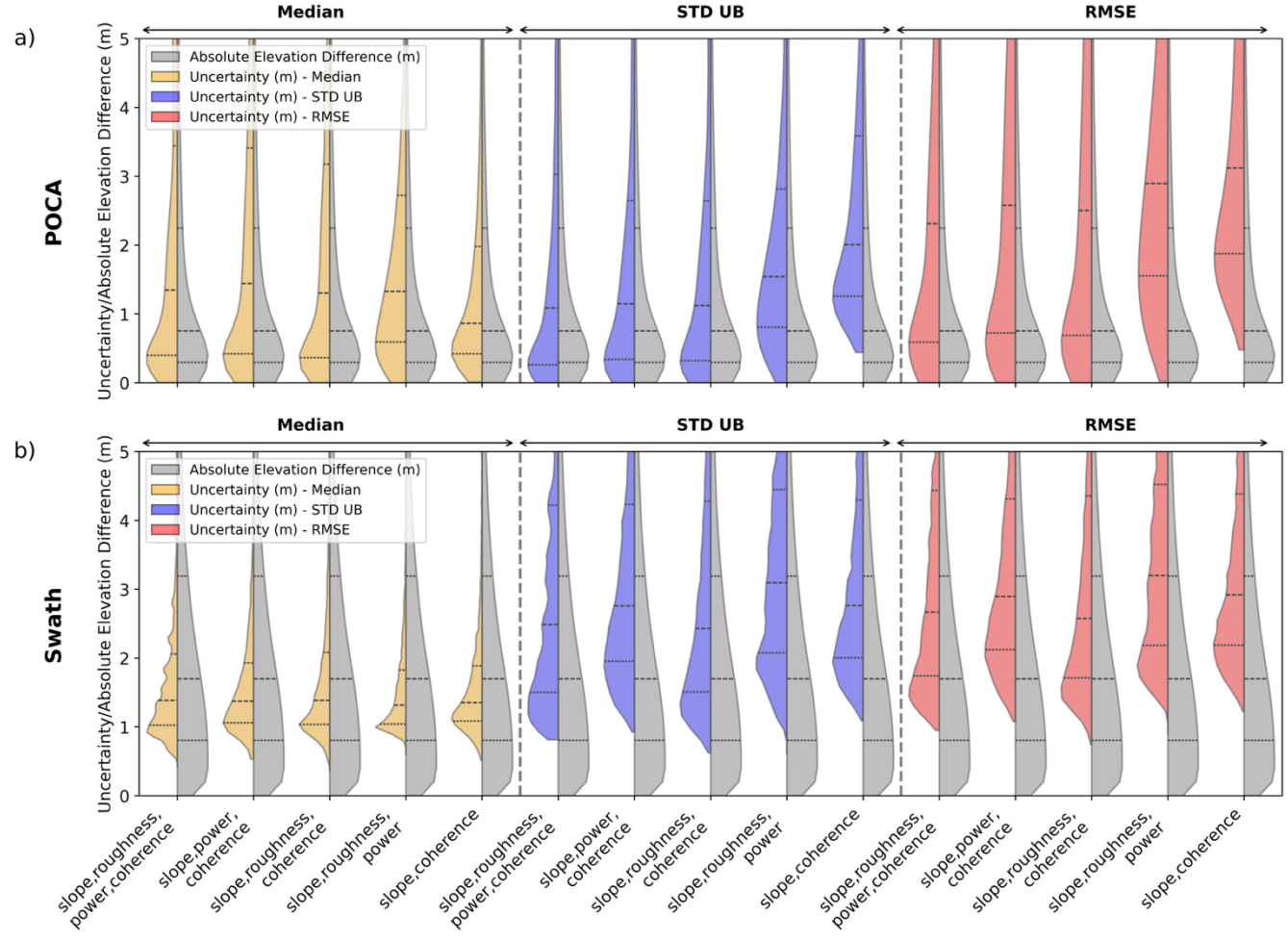

600 **Figure B4** – Comparison of the overall distributions of the absolute elevation differences relative to the reference dataset (grey) and the distribution of uncertainty values calculated using the median (yellow), STD UB (blue) and RMSE (red), for each tested method of uncertainty generation listed in Table A3, for CryoSat-2 **(a)** POCA and **(b)** swath-processed data, over the Greenland Ice Sheet SARIn region in 2022. Dashed and dotted horizontal black lines denote the median and lower/upper quartiles, respectively, of each distribution.

605

https://doi.org/10.5194/egusphere-2026-556
Preprint. Discussion started: 17 March 2026

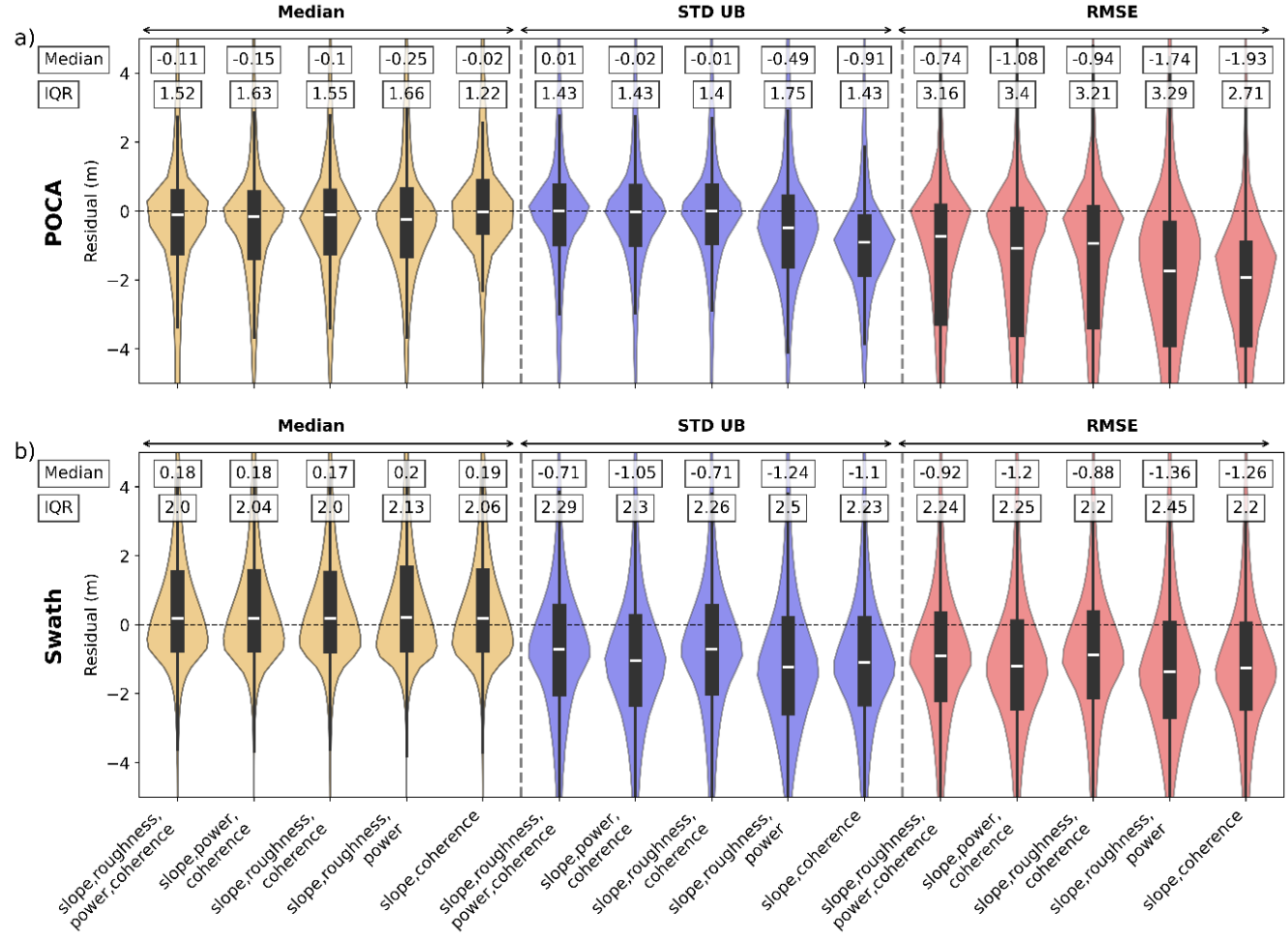

Figure B5 – Comparison of residuals (difference between uncertainty and the unseen elevation difference to a reference dataset), for each method of uncertainty generation listed in Table A3, for CryoSat-2 **(a)** POCA and **(b)** swath-processed data, over the Greenland Ice Sheet SARIn region in 2022. Residual distributions are displayed as violin plots whereby the width represents the proportion of data. Negative (positive) residuals represent cases where the uncertainty is larger (smaller) than the absolute elevation difference. Residual distributions calculated from uncertainties using the median, STD UB and RMSE are coloured yellow, blue and red, respectively. Black box plots are provided within each residual distribution, with a white horizontal line representing the median. The median and inter-quartile range (IQR) are provided for each distribution in text boxes.

https://doi.org/10.5194/egusphere-2026-556
Preprint. Discussion started: 17 March 2026

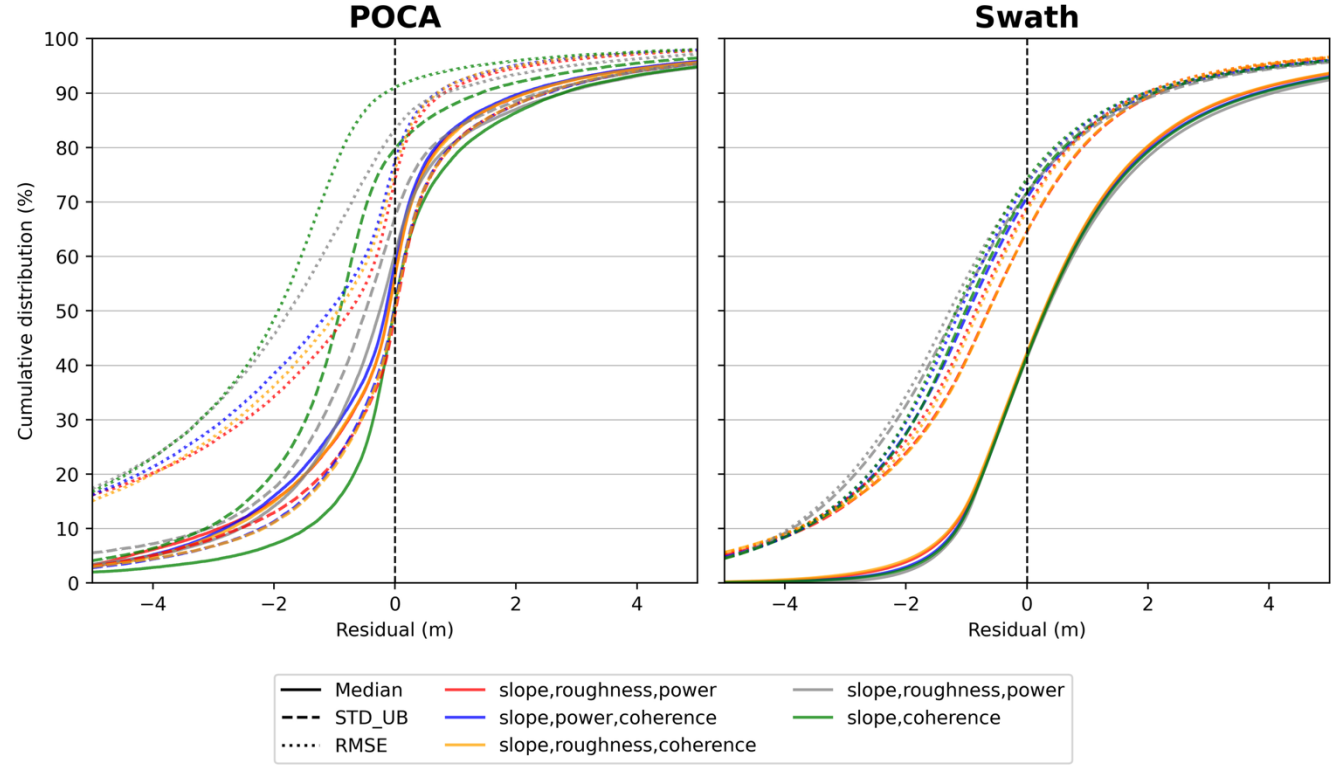

Figure B6 – Cumulative distributions of residuals (difference between uncertainty and the unseen elevation differences relative to a reference dataset), for each method of uncertainty generation for CryoSat-2-derived POCA (top) and swath-processed (bottom) data, for the Greenland Ice Sheet SARIn region in 2022.

https://doi.org/10.5194/egusphere-2026-556
Preprint. Discussion started: 17 March 2026

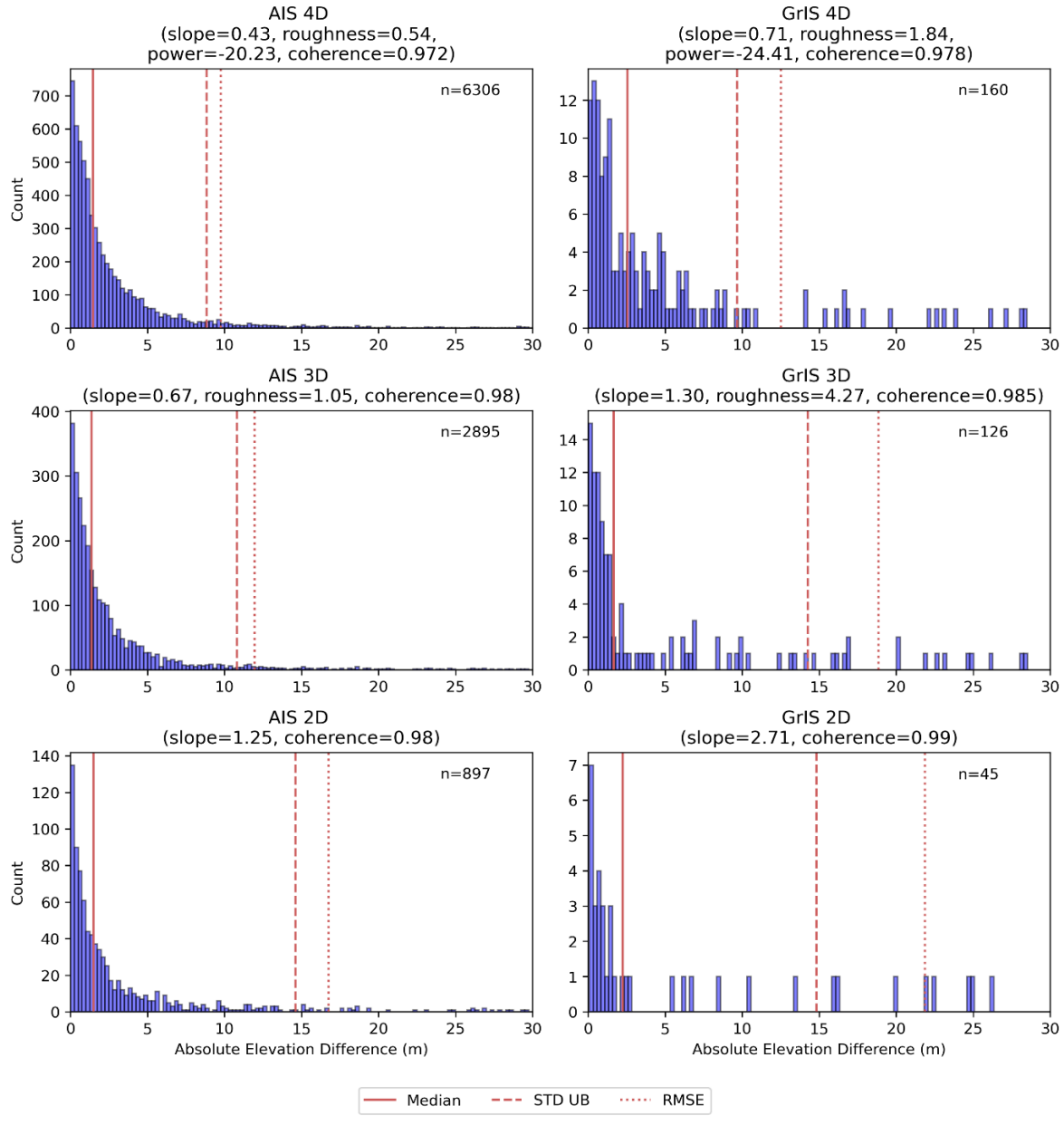

Figure B7 – Distribution of absolute elevation difference values assigned to the most populated CryoSat-2 uncertainty lookup table bins for Antarctica (left) and Greenland (right). Examples are shown for the most populated bins in four- (top row), three- (middle row) and two- (bottom row) dimensional lookup tables. The lower bound of the bin boundary for each co-variate in the lookup table is provided in the title above each panel. Solid, dashed and dotted red vertical lines represent the median, upper bound of the standard deviation (STD UB) and the root mean square error (RMSE) calculated for each distribution. The total number of absolute elevation difference values assigned to a given uncertainty lookup table bin (n) is given in the top right of each distribution.

https://doi.org/10.5194/egusphere-2026-556
Preprint. Discussion started: 17 March 2026

Data availability

Cryo-TEMPO POCA Land Ice Baseline D data are available from https://doi.org/10.5270/CR2-3205d1e; Cryo-TEMPO EOLIS data are available from https://doi.org/10.5270/CR2-2xs4q4l and both datasets can also be accessed via the cs2eo data platform at https://cs2eo.org/; ESA L2I Baseline E SARIn POCA data are available from https://doi.org/10.5270/CR2-65cff05; Sentinel-3 Level-2 Hydro-Cryo Thematic Product Baseline Collection No. 005 are available from https://doi.org/10.57780/s3d-6c5ea43; ICESat-2 ATL06 Land Ice Height v6 data are available from: https://doi.org/10.5067/ATLAS/ATL06.006.

Author contributions

KB and MM designed the study, with input from SD and NG. AM, KB, SA, SD and CW developed the code to generate and evaluate the uncertainties. KB performed all CryoSat-2 POCA and Sentinel-3 analyses, SA performed CryoSat-2 swath analyses. JP created the slope and roughness data. KB wrote the manuscript, with contributions from all co-authors.

Competing interests

The contact author has declared that none of the authors has any competing interests.

Acknowledgements

This work was supported by the European Space Agency (ESA) CRISTAL Level-2 Processor Prototype and R&D: Land Ice and Inland Water (CLEV2ER LIIW) study (Contract No. 4000141377/23/I-AG), the ESA CryoSat-2 Thematic Products (Cryo-TEMPO) study (Contract No. 4000132237/20/I-NS), and the UK Natural Environmental Research Council Centre for Polar Observation and Modelling (Grant No. NE/Y006178/1). We particularly wish to thank Michele Scagliola, Paolo Cipollini, Alessandro Di Bella and Jérôme Bouffard for actively supporting these projects. We further thank ESA for providing free access to CryoSat-2 data, the National Aeronautics and Space Administration (NASA) for providing free access to ICESat-2 data, and the Polar Geospatial Center (PGC) for providing free access to the ArcticDEM and REMA.

Financial support

This research has been supported by the European Space Agency (ESA) CRISTAL Level-2 Processor Prototype and R&D: Land Ice and Inland Water (CLEV2ER LIIW) study (Contract No. 4000141377/23/I-AG), the ESA CryoSat-2 Thematic

https://doi.org/10.5194/egusphere-2026-556
Preprint. Discussion started: 17 March 2026

Products (Cryo-TEMPO) study (Contract No. 4000132237/20/I-NS), the ESA CryoSat-2 Thematic Products (Cryo-TEMPO) Elevation Over Land Ice from Swath (EOLIS) study, the UK Natural Environmental Research Council Centre for Polar Observation and Modelling (Grant No. NE/Y006178/1), and the UK Engineering and Physical Sciences Research Council (Grant No. EP/Y02642X/1).

References

Adusumilli, S., Fricker, H.A., Medley, B., Padman, L. and Siegfried, M.R. (2020) Interannual variations in meltwater input to the Southern Ocean from Antarctic ice shelves. *Nature geoscience*, *13*(9), pp.616-620. https://doi.org/10.1038/s41561-020-0616-z

Bamber, J.L. and Bindschadler, R.A. (1997) An improved elevation dataset for climate and ice-sheet modelling: validation with satellite imagery. Annals of Glaciology, 25, pp.439-444. https://doi.org/10.3189/S0260305500014427

Bamber, J.L., Ekholm, S. and Krabill, W. (1998) The accuracy of satellite radar altimeter data over the Greenland ice sheet determined from airborne laser data. Geophysical Research Letters, 25(16), pp.3177-3180. https://doi.org/10.1029/98GL01594

Bamber, J.L., Gomez-Dans, J.L. and Griggs, J.A. (2009) A new 1 km digital elevation model of the Antarctic derived from combined satellite radar and laser data–Part 1: Data and methods. The Cryosphere, 3(1), pp.101-111. https://doi.org/10.5194/tc-3-101-2009

Brenner, A.C., DiMarzio, J.P. and Zwally, H.J. (2007) Precision and accuracy of satellite radar and laser altimeter data over the continental ice sheets. IEEE Transactions on Geoscience and Remote Sensing, 45(2), pp.321-331. https://doi.org/10.1109/TGRS.2006.887172

Brunt, K.M., Neumann, T.A. and Smith, B.E. (2019) Assessment of ICESat-2 ice sheet surface heights, based on comparisons over the interior of the Antarctic ice sheet. Geophysical Research Letters, 46(22), pp.13072-13078. https://doi.org/10.1029/2019GL084886

Brunt, K.M., Smith, B.E., Sutterley, T.C., Kurtz, N.T. and Neumann, T.A. (2021) Comparisons of satellite and airborne altimetry with ground-based data from the interior of the Antarctic ice sheet. Geophysical Research Letters, 48(2), p.e2020GL090572. https://doi.org/10.1029/2020GL090572

CryoTEMPO-EOLIS (2024) Elevation over land ice from swath: Algorithm theoretical basis document (Issue 2.3). European Space Agency. Available at: https://cryotempo-eolis.org/wp-content/uploads/2022/08/CryoTempo-ThematicProduct-ATBD_Latest.pdf

Davis, C.H. and Ferguson, A.C. (2004) Elevation change of the Antarctic ice sheet, 1995-2000, from ERS-2 satellite radar altimetry. IEEE Transactions on Geoscience and Remote Sensing, 42(11), pp.2437-2445. https://doi.org/10.1109/TGRS.2004.836789

https://doi.org/10.5194/egusphere-2026-556
Preprint. Discussion started: 17 March 2026

Davison, B.J., Hogg, A.E., Gourmelen, N., Jakob, L., Wuite, J., Nagler, T., Greene, C.A., Andreasen, J. and Engdahl, M.E. (2023) Annual mass budget of Antarctic ice shelves from 1997 to 2021. *Science Advances*, *9*(41), p.eadi0186. https://doi.org/10.1126/sciadv.adi0186

European Space Agency (2019) Cryo-TEMPO EOLIS, Version 1.0. [Dataset] https://doi.org/10.5270/CR2-2xs4q4l

European Space Agency (2023a) L2 LRM Precise Orbit. Baseline E. [Dataset] https://doi.org/10.5270/CR2-614f341

European Space Agency (2023b) L2 SARin Precise Orbit. Baseline E. [Dataset] https://doi.org/10.5270/CR2-65cff05

European Space Agency. (2025a). Sentinel-3 Level-2 Hydro-Cryo Thematic Products (Baseline Collection n°005) [Dataset]. https://doi.org/10.57780/s3d-6c5ea43

European Space Agency (2025b) Cryo-TEMPO Land Ice, Baseline D. [Dataset] https://doi.org/10.5270/CR2-3205d1e

Gardner, A.S., Moholdt, G., Scambos, T., Fahnstock, M., Ligtenberg, S., Van Den Broeke, M. and Nilsson, J. (2018) Increased West Antarctic and unchanged East Antarctic ice discharge over the last 7 years. The Cryosphere, 12(2), pp.521-547. https://doi.org/10.5194/tc-12-521-2018

Gourmelen, N., Escorihuela, M., Shepherd, A., Foresta, L., Muir, A., Garcia-Mondéjar, A., Roca, M., Baker, S.G. and Drinkwater, M.R. (2018) CryoSat-2 swath interferometric altimetry for mapping ice elevation and elevation change. Advances in Space Research, 62(6), pp.1226-1242. https://doi.org/10.1016/j.asr.2017.11.014

Gourmelen, N., Jakob, L., Holland, P.R., Dutrieux, P., Goldberg, D., Bevan, S., Luckman, A. and Malczyk, G. (2025) The influence of subglacial lake discharge on Thwaites Glacier ice-shelf melting and grounding-line retreat. Nature Communications, *16*(1), p.2272. https://doi.org/10.1038/s41467-025-57417-1

Helm, V., Humbert, A. and Miller, H. (2014) Elevation and elevation change of Greenland and Antarctica derived from CryoSat-2. The Cryosphere, 8(4), pp.1539-1559. https://doi.org/10.5194/tc-8-1539-2014

Howat I., Porter C., Noh M., Husby E., Khuvis S., Danish E., Tomko K., Gardiner J., Negrete A., Yadav B., Klassen J., Kelleher C., Cloutier M., Bakker J., Enos J., Arnold G., Bauer G., Morin P. (2022) "The Reference Elevation Model of Antarctica – Mosaics, Version 2", https://doi.org/10.7910/DVN/EBW8UC, Harvard Dataverse, V1.

Johannessen, O.M., Khvorostovsky, K., Miles, M.W. and Bobylev, L.P. (2005) Recent ice-sheet growth in the interior of Greenland. Science, 310(5750), pp.1013-1016. https://doi.org/10.1126/science.1115356

Konrad, H., Gilbert, L., Cornford, S.L., Payne, A., Hogg, A., Muir, A. and Shepherd, A. (2017) Uneven onset and pace of ice-dynamical imbalance in the Amundsen Sea Embayment, West Antarctica. Geophysical Research Letters, 44(2), pp.910-918. https://doi.org/10.1002/2016GL070733

Li, T., Dawson, G., Chuter, S. and Bamber, J. (2021) A high-resolution Antarctic grounding zone product from ICESat-2 laser altimetry. Earth System Science Data Discussions, 2021, pp.1-35. https://doi.org/10.5194/essd-14-535-2022

Malczyk, G., Gourmelen, N., Goldberg, D., Wuite, J. and Nagler, T. (2020) Repeat subglacial lake drainage and filling beneath Thwaites Glacier. Geophysical Research Letters, *47*(23), p.e2020GL089658. https://doi.org/10.1029/2020GL089658

https://doi.org/10.5194/egusphere-2026-556
Preprint. Discussion started: 17 March 2026

McMillan, M., Leeson, A., Shepherd, A., Briggs, K., Armitage, T.W., Hogg, A., Kuipers Munneke, P., van den Broeke, M., Noël, B., van de Berg, W.J. and Ligtenberg, S. (2016) A high-resolution record of Greenland mass balance. Geophysical Research Letters, 43(13), pp.7002-7010. https://doi.org/10.1002/2016GL069666

McMillan, M., Shepherd, A., Sundal, A., Briggs, K., Muir, A., Ridout, A., Hogg, A. and Wingham, D. (2014) Increased ice losses from Antarctica detected by CryoSat-2. Geophysical Research Letters, 41(11), pp.3899-3905. https://doi.org/10.1002/2014GL060111

McMillan, M., Muir, A., Shepherd, A., Escolà, R., Roca, M., Aublanc, J., Thibaut, P., Restano, M., Ambrozio, A. and Benveniste, J. (2019) Sentinel-3 delay-Doppler altimetry over Antarctica. The Cryosphere, 13(2), pp.709-722. https://doi.org/10.5194/tc-13-709-2019

Moon, T., Joughin, I., Smith, B. and Howat, I. (2012) 21st-century evolution of Greenland outlet glacier velocities. Science, 336(6081), pp.576-578. https://doi.org/10.1126/science.1219985

Mouginot, J., Rignot, E., Scheuchl, B. and Millan, R. (2017) Comprehensive annual ice sheet velocity mapping using Landsat-8, Sentinel-1, and RADARSAT-2 data. Remote Sensing, 9(4), p.364. https://doi.org/10.3390/rs9040364

Nilsson, J., Gardner, A.S. and Paolo, F.S. (2022) Elevation change of the Antarctic Ice Sheet: 1985 to 2020. *Earth System Science Data*, *14*(8), pp.3573-3598. https://doi.org/10.5194/essd-14-3573-2022

Otosaka, I.N., Shepherd, A., Ivins, E.R., Schlegel, N.J., Amory, C., van den Broeke, M., Horwath, M., Joughin, I., King, M., Krinner, G. and Nowicki, S. (2022) Mass balance of the Greenland and Antarctic ice sheets from 1992 to 2020. Earth System Science Data Discussions, 2022, pp.1-33. https://doi.org/10.5194/essd-15-1597-2023

Phillips, J. and McMillan, M. (2024) Assessment of Sentinel-3 Altimeter Performance over Antarctica using High Resolution Digital Elevation Models. EGUsphere, 2024, pp.1-26. https://doi.org/10.5194/egusphere-2024-3054

Porter, C., Howat, I., Noh, M.J., Husby, E., Khuvis, S., Danish, E., Tomko, K., Gardiner, J., Negrete, A., Yadav, B., Klassen, J., Kelleher, C., Cloutier, M., Bakker, J., Enos, J., Arnold, G., Bauer, G., and Morin, P. (2023) "ArcticDEM – Mosaics, Version 4.1", https://doi.org/10.7910/DVN/3VDC4W, Harvard Dataverse, V1.

Remy, F., Mazzega, P., Houry, S., Brossier, C. and Minster, J.F. (1989) Mapping of the topography of continental ice by inversion of satellite-altimeter data. Journal of Glaciology, 35(119), pp.98-107. https://doi.org/10.3189/002214389793701419

Sasgen, I., Wouters, B., Gardner, A.S., King, M.D., Tedesco, M., Landerer, F.W., Dahle, C., Save, H. and Fettweis, X. (2020) Return to rapid ice loss in Greenland and record loss in 2019 detected by the GRACE-FO satellites. Communications Earth & Environment, 1(1), p.8. https://doi.org/10.1038/s43247-020-0010-1

Schröder, L., Horwath, M., Dietrich, R., Helm, V., Van Den Broeke, M.R. and Ligtenberg, S.R. (2019) Four decades of Antarctic surface elevation changes from multi-mission satellite altimetry. The Cryosphere, 13(2), pp.427-449. https://doi.org/10.5194/tc-13-427-2019

https://doi.org/10.5194/egusphere-2026-556
Preprint. Discussion started: 17 March 2026

Shepherd, A., Gilbert, L., Muir, A.S., Konrad, H., McMillan, M., Slater, T., Briggs, K.H., Sundal, A.V., Hogg, A.E. and Engdahl, M.E. (2019) Trends in Antarctic Ice Sheet elevation and mass. Geophysical Research Letters, 46(14), pp.8174-8183. https://doi.org/10.1029/2019GL082182

Shepherd, A., Ivins, E.R., A, G., Barletta, V.R., Bentley, M.J., Bettadpur, S., Briggs, K.H., Bromwich, D.H., Forsberg, R., Galin, N. and Horwath, M. (2012) A reconciled estimate of ice-sheet mass balance. Science, 338(6111), pp.1183-1189. https://doi.org/10.1126/science.1228102

Siegfried, M.R. and Fricker, H.A. (2018) Thirteen years of subglacial lake activity in Antarctica from multi-mission satellite altimetry. Annals of Glaciology, 59(76pt1), pp.42-55. https://doi.org/10.1017/aog.2017.36

Sørensen, L.S., Simonsen, S.B., Meister, R., Forsberg, R., Levinsen, J.F. and Flament, T. (2015) Envisat-derived elevation changes of the Greenland ice sheet, and a comparison with ICESat results in the accumulation area. Remote Sensing of Environment, 160, pp.56-62. https://doi.org/10.1016/j.rse.2014.12.022

Smith, B.E., Gourmelen, N., Huth, A. and Joughin, I. (2017) Connected subglacial lake drainage beneath Thwaites glacier, west Antarctica. The Cryosphere, 11(1), pp.451-467. https://doi.org/10.5194/tc-11-451-2017

Smith, B., S. Adusumilli, B. M. Csathó, D. Felikson, H. A. Fricker, A. Gardner, N. Holschuh, J. Lee, F. S. Paolo, M. R. Siegfried, T. Sutterley and the ICESat-2 Science Team (2023) ATLAS/ICESat-2 L3A Land Ice Height, Version 6.. Boulder, Colorado USA. NASA National Snow and Ice Data Center Distributed Active Archive Center. https://doi.org/10.5067/ATLAS/ATL06.006

Suryawanshi, M.R., McMillan, M., Maddalena, J., Piras, F., Aublanc, J., Daguzé, J.A., Grau, C. and Huang, Q. (2025) New radar altimetry datasets of Greenland and Antarctic surface elevation, 1991–2012. The Cryosphere, 19(8), pp.2855-2880. https://doi.org/10.5194/tc-19-2855-2025

Tapley, B.D., Watkins, M.M., Flechtner, F., Reigber, C., Bettadpur, S., Rodell, M., Sasgen, I., Famiglietti, J.S., Landerer, F.W., Chambers, D.P. and Reager, J.T. (2019) Contributions of GRACE to understanding climate change. Nature climate change, 9(5), pp.358-369. https://doi.org/10.1038/s41558-019-0456-2

The IMBIE team. Mass balance of the Antarctic Ice Sheet from 1992 to 2017 (2018) Nature 558, 219–222. https://doi.org/10.1038/s41586-018-0179-y

The IMBIE Team. Mass balance of the Greenland Ice Sheet from 1992 to 2018 (2020) Nature 579, 233–239. https://doi.org/10.1038/s41586-019-1855-2

Velicogna, I., Mohajerani, Y., A, G., Landerer, F., Mouginot, J., Noel, B., Rignot, E., Sutterley, T., van den Broeke, M., van Wessem, M. and Wiese, D. (2020) Continuity of ice sheet mass loss in Greenland and Antarctica from the GRACE and GRACE follow-on missions. Geophysical Research Letters, 47(8), p.e2020GL087291. https://doi.org/10.1029/2020GL087291

Wilson, S.F., Hogg, A.E., Rigby, R., Gourmelen, N., Nias, I. and Slater, T. (2025) Detection of 85 new active subglacial lakes in Antarctica from a decade of CryoSat-2 data. Nature Communications, 16(1), p.8311. https://doi.org/10.1038/s41467-025-63773-9

https://doi.org/10.5194/egusphere-2026-556
Preprint. Discussion started: 17 March 2026

Wingham, D.J., Shepherd, A., Muir, A. and Marshall, G.J. (2006a) Mass balance of the Antarctic ice sheet. Philosophical Transactions of the Royal Society A: Mathematical, Physical and Engineering Sciences, 364(1844), pp.1627-1635. https://doi.org/10.1098/rsta.2006.1792

Wingham, D.J., Francis, C.R., Baker, S., Bouzinac, C., Brockley, D., Cullen, R., de Chateau-Thierry, P., Laxon, S.W., Mallow, U., Mavrocordatos, C. and Phalippou, L. (2006b) CryoSat: A mission to determine the fluctuations in Earth's land and marine ice fields. *Advances in Space Research*, *37*(4), pp.841-871. https://doi.org/10.1016/j.asr.2005.07.027

Zwally, H.J., Li, J., Brenner, A.C., Beckley, M., Cornejo, H.G., DiMARZIO, J., Giovinetto, M.B., Neumann, T.A., Robbins, J., Saba, J.L. and Yi, D. (2011) Greenland ice sheet mass balance: distribution of increased mass loss with climate warming; 2003–07 versus 1992–2002. Journal of Glaciology, 57(201), pp.88-102. https://doi/org/10.3189/002214311795306682